

Stress analysis of polycrystalline thin films and surface regions by X-ray diffraction

U. Welzel,^{a*} J. Ligot,^a P. Lamparter,^a A. C. Vermeulen^b and E. J. Mittemeijer^a

Received 14 April 2004

Accepted 12 November 2004

^aMax Planck Institute for Metals Research, Heisenbergstr. 3, 70569 Stuttgart, Germany, and^bPANalytical, Lelyweg 1, 7602 EA Almelo, The Netherlands. Correspondence e-mail:

u.welzel@mf.mpg.de

The components of the macroscopic mechanical stress tensor of a stressed thin film, coating, multilayer or the region near the surface of a bulk material can in principle be determined by X-ray diffraction. The various analysis methods and measurement strategies, in dependence on specimen and measurement conditions, are summarized and evaluated in this paper. First, different X-ray diffraction geometries (conventional or grazing incidence) are described. Then, the case of macroscopically elastically isotropic, untextured specimens is considered: from the simplest case of a uniaxial state of stress to the most complicated case of a triaxial state of stress. The treatment is organized according to the number of unknowns to be determined (*i.e.* the state of stress, principal axes known or unknown), the use of one or several values of the rotation angle φ and the tilt angle ψ of the sample, and one or multiple hkl reflections. Next, the focus is on macroscopically elastically anisotropic (*e.g.* textured) specimens. In this case, the use of diffraction (X-ray) elastic constants is not possible. Instead, diffraction (X-ray) stress factors have to be used. On the basis of examples, it is demonstrated that successful diffraction stress analysis is only possible if an appropriate grain-interaction model is applied.

© 2005 International Union of Crystallography
Printed in Great Britain – all rights reserved

1. Introduction

In thin films and regions near the surface of bulk materials, residual stresses are generally present (see, for example, Hoffman, 1966, 1976; Windischmann, 1992; Machlin, 1995; *Proceedings of the International Conference on Residual Stresses, Proceedings of the European Conference on Residual Stresses*). The analysis of the residual stress state is of great technological importance because stresses can be beneficial or detrimental with respect to, in particular, the mechanical properties (see, for example, Hauk, 1997, §6 therein). As an example, stress can result in cracking of a film in the case of tensile stress, or buckling in the case of compressive stress. If, on the other hand, a film or surface layer can be pre-stressed during its production, a compressive pre-stress may prevent cracking when stresses resulting from external forces occur during service life.

Among a number of methods available for stress analysis, X-ray diffraction methods employing the characteristic radiation emitted from an X-ray tube or medium-energy synchrotron radiation ($E = 5\text{--}15$ keV) are very suitable for the analysis of films and surface layers. The rather limited penetration depth of (such) X-rays in solid matter results in surface sensitivity. X-ray diffraction methods allow a determination of the full mechanical stress tensor of all crystalline phases; furthermore, the analysis of stress gradients is feasible. Moreover, useful additional information can be obtained as a

by-product of X-ray diffraction stress measurements: whereas the stress analysis uses the shifts of diffraction lines, the (integral) intensities of diffraction lines contain information on the crystallographic texture (see, for example, Bunge, 1982), and the shapes and breadths of diffraction lines contain information on the size (distribution) of diffracting domains and the content of crystalline defects such as dislocations and stacking faults (see, for example, Delhez *et al.*, 1982).

In principle, no distinction exists between the analysis of stress in bulk materials and in thin layers. However, dedicated diffraction geometries for films much thinner than the X-ray penetration depth have been developed in the past few years and thin films are frequently mechanically elastically anisotropic due to the occurrence of crystallographic texture and/or direction-dependent grain interaction¹ (Welzel & Mittemeijer, 2003). Thus, standard methods of analysis applicable to bulk aggregates [*e.g.* the traditional $\sin^2\psi$ analysis employing diffraction (X-ray) elastic constants] may fail when applied to the stress analysis of thin films (see, for example, van Leeuwen *et al.*, 1999; Leoni *et al.*, 2001; Welzel *et al.*, 2003; Welzel, Leoni & Mittemeijer, 2004). New developments dedicated to the stress analysis of thin films and surface layers are a focal point of interest in this review paper.

¹ The notion 'direction-dependent grain interaction' signifies that different grain-interaction assumptions prevail along different directions in the specimen.

Table 1

Review articles on diffraction stress analysis with a short description of the contents according to various categories.

Reference	Focus	Fundamentals	Instrumentation	Analysis of gradients	Elastically quasi-isotropic case	Elastically anisotropic case (case of texture)	Comments
Noyan <i>et al.</i> (1995)	Thin-film stress analysis by X-ray diffraction; polycrystalline and epitaxial films	Origins of stress; types of residual stresses (macro <i>versus</i> micro); stress states of thin films	Brief treatment of traditional (Bragg–Brentano, Seeman–Bohlin) and high-resolution diffractometers; microbeam diffraction	Grazing/glancing-incidence diffraction	Basic treatment	–	Also covered: stress from curvature measurements, reflectometry for determination of film thickness and composition
Eigenmann & Macherauch (1995)	Stress analysis by X-ray diffraction; poly- and single-crystalline specimens	Historical review; types of residual stresses (macro <i>versus</i> micro)	Detailed treatment of laboratory (Bragg–Brentano) and portable diffractometers	–	Full treatment; calculation of X-ray elastic constants	–	Sequence of four publications in German; introduction with historical review
Hauk (1995)	Stress analysis by X-ray and neutron diffraction; polycrystalline specimens	Brief introduction	Brief introduction	Brief introduction	Brief introduction	Only mentioned; no details	In German
Dölle (1979)	Stress analysis by X-ray diffraction; polycrystalline specimens	Brief introduction and brief historical review	–	Effect of a stress gradient on a $\sin^2 \psi$ analysis is discussed	Full treatment; calculation of X-ray elastic constants	Simplified treatment (assuming a Reuss-type grain interaction)	

A selection of reviews on X-ray diffraction stress analysis in the past 25 years is given in Table 1. Only reviews with a general scope, *i.e.* reviews not only dedicated to a certain class of materials (*e.g.* ceramics, metals or polymers), have been included. The listing is not complete but embodies a representative collection. Inspection of the existing literature shows that earlier reviews are either incomplete or superficial, in particular in view of the indicated new developments. A practical systematization and a balanced presentation of the determination of the state of stress for macroscopically elastically *isotropic versus anisotropic* bodies is lacking. Further, a review on stress analysis of thin films should at least mention methods of analysis applicable to textured polycrystals, as texture is met frequently in thin films. It is indispensable, in this case, to at least mention the use of diffraction (X-ray) stress factors and the use of the crystallite group method, and yet previous reviews that focused on the case of thin films did not deal with these aspects.

The present work reviews the various methods of (X-ray) diffraction analysis of macroscopic mechanical stress states. For this reason, methods for the analysis of local stresses down to the submicrometre scale by microdiffraction employing synchrotron radiation, a rapidly developing field of research (see, for example, Tamura *et al.*, 2003, and references therein), have been excluded. These methods require dedicated diffraction apparatus (*e.g.* white-beam synchrotron radiation, two-dimensional detectors) as well as dedicated methods of analysis. Further, the analysis of microstresses/strains from diffraction line broadening has been excluded (see, for example, Mittemeijer & Scardi, 2004). The purely technical aspects (such as the selection of X-ray optics, the selection of X-ray counters, *etc.*) of the stress measurement, as well as the determination of the position of diffraction lines (*i.e.* the

maximum or centroid of a diffraction line), are not treated. For details, the reader is referred to, for example, Hauk (1997, §§2.04 and 2.05 therein). Measurement strategies for stress analysis at fixed information depth are discussed, but the calculation of stress depth profiles from such measurements exceeds the scope of this paper and has been excluded (for an example, see Somers & Mittemeijer, 1990).

Special attention is paid to the determination of stress in thin films. Recipes are given that allow direct practical application of traditional and new methods. The paper is organized as follows. The theoretical, general equations for the stress analysis of macroscopically elastically isotropic and anisotropic polycrystals are presented in §2. The different diffraction geometries (modes of sample rotation, conventional and grazing-incidence diffraction) are briefly described in §3. The practical methods of stress analysis for *macroscopically elastically isotropic* polycrystals have been gathered in §4. These methods are tailored for specific states of stresses, in such a way that they allow the direct determination of the stress tensor components from simple linear regressions in plots of measured lattice strains. The practical methods of stress analysis for *macroscopically elastically anisotropic* specimens (*i.e.* of specimens possessing crystallographic texture and/or direction-dependent grain interaction) are dealt with in §5.

Different grain-interaction models, enabling the calculation of diffraction (X-ray) elastic constants and diffraction (X-ray) stress factors from single-crystal elastic data, are presented in Appendix A.

2. Theoretical background

In the absence of external loads, stresses present in the sample are called residual stresses. Three additive kinds of residual

stresses in a polycrystalline material are distinguished according to their corresponding length scales (Macherauch *et al.*, 1973; see also Noyan *et al.*, 1995):

$$\sigma^{\text{RS}} = \sigma_{\text{I}}^{\text{RS}} + \sigma_{\text{II}}^{\text{RS}} + \sigma_{\text{III}}^{\text{RS}}, \quad (1)$$

where $\sigma_{\text{I}}^{\text{RS}}$ represents the average of the residual stresses over many grains. $\sigma_{\text{II}}^{\text{RS}}$ is defined as the difference between the average of the residual stresses over a particular grain and $\sigma_{\text{I}}^{\text{RS}}$. $\sigma_{\text{III}}^{\text{RS}}$ represents the deviation of the local stress σ^{RS} in a particular grain from the average stress in the grain. In the present work, only the determination of the macro-residual stress $\sigma_{\text{I}}^{\text{RS}}$ is dealt with. For origins of residual stresses in thin films, see *e.g.* the review by Windischmann (1992) and many references therein.

2.1. Concept of diffraction stress analysis

The basic idea is sketched in Fig. 1, where it is assumed that a polycrystalline specimen is subjected to a compressive stress parallel to the surface. Due to the presence of stress, the lattice spacing of the hkl lattice planes in a crystallite depends on the orientation of the crystallite in the specimen with respect to the specimen frame of reference. With X-ray diffraction analysis, direction-dependent measurement of (elastic) lattice strains is possible. Bragg's law,

$$\lambda = 2d^{\text{hkl}} \sin \theta^{\text{hkl}}, \quad (2)$$

relates the lattice spacing d^{hkl} of the planes with Laue indices hkl to the diffraction angle $2\theta^{\text{hkl}}$ and the wavelength λ . Note that the lattice spacing is measured in the direction of the diffraction vector. Usually the diffraction angle $2\theta^{\text{hkl}}$ (a fixed value for one reflection) is obtained from the position of the maximum or centroid of the hkl diffraction line. Then it is possible to calculate the elastic strain of the $\{hkl\}$ planes from

$$\varepsilon^{\text{hkl}} = (d^{\text{hkl}} - d_0^{\text{hkl}})/d_0^{\text{hkl}}, \quad (3)$$

where d_0^{hkl} is the strain-free lattice spacing of the $\{hkl\}$ lattice planes. The direction of the strain measurement, *i.e.* the direction of the diffraction vector, is usually identified by the

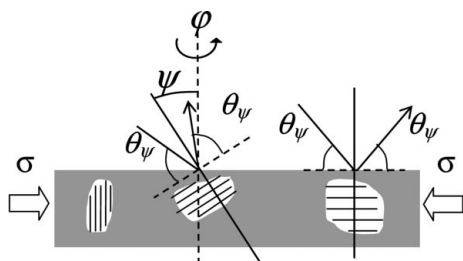


Figure 1

Concept of diffraction stress analysis. When a polycrystal is subjected to stress (in this case a uniaxial compression parallel to the surface), the lattice spacing of the hkl lattice planes varies with the orientation of the lattice planes with respect to the loading direction. This direction-dependent lattice strain can be measured by X-ray diffraction. The direction of the strain measurement is the direction of the diffraction vector and is identified by the angles φ and ψ , where φ is the rotation angle of the specimen about the specimen surface normal and ψ is the inclination angle of the specimen surface normal with respect to the diffraction vector.

angles φ and ψ , where ψ is the angle of inclination of the specimen surface normal with respect to the diffraction vector and φ denotes the rotation of the specimen around the specimen surface normal (see Fig. 2).

A diffraction line contains information on the elastic strain of crystallites only for such crystallites which have their $\{hkl\}$ planes oriented perpendicular to the diffraction vector, *i.e.* only the elastic strain of a subgroup of crystallites composing a polycrystalline specimen is analysed in a lattice-strain measurement. In general, the strain measured by X-ray diffraction is not equal to the mechanical strain in the same direction, characterized by (φ, ψ) , as the mechanical strain is an average over all crystallites in the sample, whereas the diffraction strain represents only a subgroup of the crystallites composing the sample. Thus, it is of paramount importance in diffraction stress analysis to distinguish diffraction averages, *e.g.* the diffraction strain for a given reflection hkl in a given direction, from the mechanical average strain in the same direction.

Basic equations for the handling of tensorial quantities (like strain and stress tensors) in the various appropriate frames of reference, and the corresponding mechanical and diffraction averages, also in the case of preferred orientation (texture), are summarized in the following.

2.2. Frames of reference for diffraction stress analysis

The following Cartesian reference frames will be distinguished (see also Fig. 2).

The crystal reference frame (C): In general, a convention for the definition of an orthonormal crystal system, such as that given by Nye (1957) (for a detailed treatment, see also Giacobozzo *et al.*, 1998), has to be adopted. For cubic crystal symmetry, the axes are chosen to coincide with the a , b and c axes of the crystal lattice.

The specimen reference frame (S): The S_3 axis is oriented perpendicular to the specimen surface and the S_1 and S_2 axes

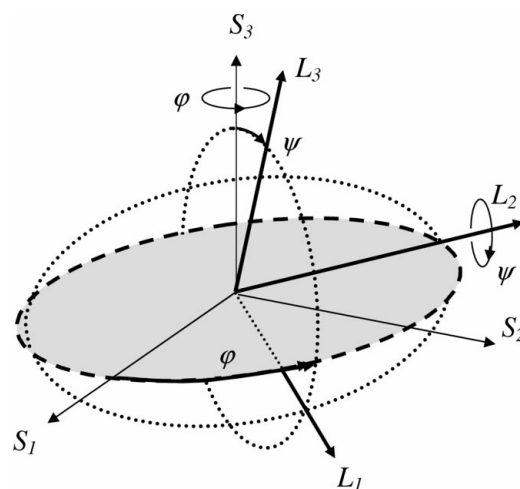


Figure 2

Definition of, and relations between, the sample (S) and laboratory (L) reference frames.

lie in the surface plane. If a preferred direction within the plane of the surface exists, *e.g.* the rolling direction in the case of a rolled specimen, the S_1 direction is usually oriented along this preferred direction. A special specimen frame of reference is the *principal reference frame* (of the stress tensor) (P). In this reference frame, only the following components of the stress tensor are non-zero: σ_{11} , σ_{22} and σ_{33} .

The laboratory reference frame (L): This frame is chosen in such a way that the L_3 axis coincides with the diffraction vector. For $\varphi = \psi = 0$, the laboratory frame of reference coincides with the specimen frame of reference.

In the following, a superscript [C, S (P) or L] is used to indicate the reference frame adopted for the representation of tensors. The absence of any superscript implies the validity of an equation independent of the reference frame used for tensor representation, but the same reference frame has to be adopted for all tensors within the equation concerned. For the relative orientation of the specimen and laboratory reference frames with respect to each other, see Fig. 2.

Transformations of tensors (from one frame of reference to another one) can be accomplished by suitable rotation matrices describing the spatial relations between the frames of reference concerned [for a general introduction to the use of transformation matrices in the context of diffraction stress analysis, see, for example, Noyan & Cohen (1987) and Hauk (1997)].

2.3. Crystallographic texture and the orientation distribution function (ODF)

The orientation of each crystallite in the S system can be identified by three Euler angles. The convention of Roe & Krigbaum (1964) in the definition of these angles will be adopted and these angles will be called α , β and γ . The set of Euler angles (α, β, γ) can be associated with a vector $\mathbf{g} = (\alpha, \beta, \gamma)$ in the three-dimensional orientation (Euler) space G [for a detailed treatment the reader is referred to *e.g.* Bunge (1982)]. In this way, each point in the orientation space represents a possible orientation of the C reference frame (for the crystallite concerned) with respect to the S reference frame. In the absence of texture, it holds that the volume fraction of crystallites having an orientation in the infinitesimal orientation range $d^3g = \sin(\beta) d\alpha d\beta d\gamma$ around \mathbf{g} is independent of \mathbf{g} . Texture can be quantified by introducing the so-called orientation distribution function (ODF), $f(\alpha, \beta, \gamma)$, specifying the volume fraction of crystallites having an orientation in the infinitesimal orientation range $d^3g = \sin(\beta) d\alpha d\beta d\gamma$ around \mathbf{g} :

$$\frac{dV(\mathbf{g})}{V} = \frac{f(\mathbf{g})}{8\pi^2} d^3g = \frac{f(\alpha, \beta, \gamma)}{8\pi^2} \sin(\beta) d\alpha d\beta d\gamma \quad (4)$$

with

$$\int_G \int_G \int_G [f(\mathbf{g})/8\pi^2] d^3g = 1. \quad (5)$$

2.4. Tensor averages (mechanical and diffraction averages)

Mechanical and diffraction averages of stress and strain tensors are usually calculated in Euler space G. In the

following, angular brackets $\langle \dots \rangle$ denote averages of a tensor Ω (*e.g.* the strain tensor) for all crystallites in the aggregate considered, *i.e.* mechanical averages:

$$\begin{aligned} \langle \Omega \rangle &= \frac{1}{8\pi^2} \int_G \int_G \int_G \Omega(\mathbf{g}) f(\mathbf{g}) d^3g \\ &= \frac{1}{8\pi^2} \int_{\gamma=0}^{2\pi} \int_{\beta=0}^{\pi} \int_{\alpha=0}^{2\pi} \Omega(\alpha, \beta, \gamma) f(\alpha, \beta, \gamma) \sin(\beta) d\alpha d\beta d\gamma. \end{aligned} \quad (6)$$

In equation (6), $\Omega(\alpha, \beta, \gamma)$ has to be understood as an average for all grains with a particular orientation in a specimen.

Braces $\{ \dots \}$ denote averages of a tensor Ω (*e.g.* the strain tensor) for diffracting crystallites only, *i.e.* diffraction averages. A diffraction line contains data on only a subset of the crystallites for which the diffracting planes are perpendicular to the chosen measurement direction. A degree of freedom occurs for the diffracting crystallites: the rotation around the diffraction vector (denoted by the angle λ in the following). In a diffraction measurement, the subset of diffracting crystallites is selected by hkl of the reflection considered and the orientation of the diffraction vector with respect to the specimen reference frame, which is indicated by the two angles φ and ψ . These quantities, selecting the ensemble of crystallites for an diffraction average, are attached to the corresponding average as sub- (φ, ψ) and superscripts (hkl):

$$\{\Omega\}_{\varphi, \psi}^{hkl} = \frac{\int_0^{2\pi} \Omega(hkl, \lambda, \varphi, \psi) f^*(hkl, \lambda, \varphi, \psi) d\lambda}{\int_0^{2\pi} f^*(hkl, \lambda, \varphi, \psi) d\lambda} \quad (7)$$

$f^*(hkl, \lambda, \varphi, \psi)$ is the representation of the ODF in terms of the measurement parameters and the rotation angle λ . The ODF as defined in equation (4) cannot be directly used in equation (7) in analogy to equation (6) since the angles λ, φ, ψ are not Euler angles representing a rotation of the C system with respect to the S system (they provide the rotation of the system L with respect to the system S). However, the values of α, β, γ and thus $f(\alpha, \beta, \gamma)$ at every λ can be calculated from hkl, λ, φ and ψ , to be finally substituted for $f^*(hkl, \lambda, \varphi, \psi)$ in equation (7) [for a more detailed treatment of the necessary transformations, see Leoni *et al.* (2001)]. Thus, the diffraction strain $\varepsilon_{\varphi\psi}^{hkl}$ can be calculated as the average strain $\{\varepsilon_{33}^L\}_{\varphi\psi}^{hkl}$, *i.e.* the strain parallel to the L_3 axis:

$$\varepsilon_{\varphi\psi}^{hkl} = \{\varepsilon_{33}^L\}_{\varphi\psi}^{hkl} = \frac{\int_0^{2\pi} \varepsilon_{33}^L(hkl, \lambda, \varphi, \psi) f^*(hkl, \lambda, \varphi, \psi) d\lambda}{\int_0^{2\pi} f^*(hkl, \lambda, \varphi, \psi) d\lambda}. \quad (8)$$

2.5. The basic equations of diffraction stress analysis

2.5.1. Elastically isotropic specimens. The simplest specimen for diffraction stress analysis is a polycrystal composed of (individually) elastically isotropic crystallites. The basic principle of the method will be discussed for such a specimen first, before the more complicated effects of single-crystal elastic anisotropy, in combination with direction-dependent grain interaction (*cf.* Appendix A) and texture, are introduced.

For a polycrystal composed of elastically isotropic crystallites, Hooke's law relating the mechanical strain to the mechanical stress tensor reads (see, for example, Meyers & Chawla, 1984):

$$\begin{aligned} \langle \varepsilon_{ij}^S \rangle &= S_{ijkl}^S \langle \sigma_{kl}^S \rangle = S_{ijkl}^C \langle \sigma_{kl}^S \rangle \\ &= [S_1 \delta_{ij} \delta_{kl} + \frac{1}{2} S_2 \frac{1}{2} (\delta_{ik} \delta_{jl} + \delta_{il} \delta_{jk})] \langle \sigma_{kl}^S \rangle. \end{aligned} \quad (9)$$

Note that the Einstein convention, *i.e.* summation over indices appearing twice in a formula, is adopted throughout the paper. S_{ijkl}^S is the compliance tensor of the body referred to the specimen reference frame and can be equated to S^C , as the individual crystallites are elastically isotropic (*i.e.* all crystallites present identical elastic properties in any arbitrary frame of reference). S_1 and $\frac{1}{2} S_2$ are the only independent components of S^C . Equation (9) holds for the macroscopic body, but it also holds, in the case considered, for every crystallite in the aggregate and thus also for the strain probed by X-ray diffraction. Only in this case, all averages of tensors are equal to the corresponding tensors of the individual crystallites; thus all braces (for diffraction averages) and brackets (for mechanical averages) could be skipped. The elastic constants S_1 and $\frac{1}{2} S_2$ can be related to Young's modulus E and Poisson's ratio ν of the body:

$$S_1 = -\nu/E \quad (10)$$

and

$$\frac{1}{2} S_2 = (1 + \nu)/E. \quad (11)$$

The elastic strain $\varepsilon_{\varphi\psi}^{hkl}$ measured by X-ray diffraction is obtained from equation (8). In this particular case, no averaging is necessary as the strain tensor is identical for all crystallites:

$$\varepsilon_{\varphi\psi}^{hkl} = \{\varepsilon_{33}^L\}_{\varphi\psi}^{hkl} = \varepsilon_{33}^L = \langle \varepsilon_{33}^L \rangle. \quad (12)$$

$\langle \varepsilon_{33}^L \rangle$ can be calculated from the strain tensor in the specimen frame of reference, ε^S , and the unit vector, \mathbf{m}^S , in the direction of the diffraction vector as expressed in the specimen frame of reference as follows:

$$\begin{aligned} \varepsilon_{\varphi\psi}^{hkl} &= \langle \varepsilon_{33}^L \rangle = m_i^S \langle \varepsilon_{ij}^S \rangle m_j^S \\ &= \langle \varepsilon_{11}^S \rangle \cos^2 \varphi \sin^2 \psi + \langle \varepsilon_{22}^S \rangle \sin^2 \varphi \sin^2 \psi + \langle \varepsilon_{33}^S \rangle \cos^2 \varphi \\ &\quad + \langle \varepsilon_{12}^S \rangle \sin(2\varphi) \sin^2 \psi + \langle \varepsilon_{13}^S \rangle \cos \varphi \sin(2\psi) \\ &\quad + \langle \varepsilon_{23}^S \rangle \sin \varphi \sin(2\psi), \end{aligned} \quad (13)$$

where

$$\mathbf{m}^S = \begin{pmatrix} \sin \psi \cos \varphi \\ \sin \psi \sin \varphi \\ \cos \psi \end{pmatrix}. \quad (14)$$

By substitution of $\langle \varepsilon_{ij}^S \rangle$ in equation (13) using equation (9), the so-called $\sin^2 \psi$ law, relating the diffraction strain to the components of the mechanical stress tensor expressed in the specimen frame of reference, follows in a straightforward manner:

$$\begin{aligned} \varepsilon_{\varphi\psi}^{hkl} &= \frac{1}{2} S_2 \sin^2 \psi [\langle \sigma_{11}^S \rangle \cos^2 \varphi + \langle \sigma_{12}^S \rangle \sin(2\varphi) + \langle \sigma_{22}^S \rangle \sin^2 \varphi] \\ &\quad + \frac{1}{2} S_2 [\langle \sigma_{13}^S \rangle \cos \varphi \sin(2\psi) + \langle \sigma_{23}^S \rangle \sin \varphi \sin(2\psi) \\ &\quad + \langle \sigma_{33}^S \rangle \cos^2 \varphi] + S_1 (\langle \sigma_{11}^S \rangle + \langle \sigma_{22}^S \rangle + \langle \sigma_{33}^S \rangle). \end{aligned} \quad (15)$$

Equation (15) holds for the diffraction strain, $\varepsilon_{\varphi\psi}^{hkl}$, as well as for the mechanical strain, $\langle \varepsilon_{33}^L \rangle$. Note that, for a polycrystalline aggregate, subjected to a homogeneous stress field and consisting of elastically isotropic crystallites, equation (15) holds also in the presence of crystallographic texture and/or direction-dependent grain interaction.

The name of equation (15), ' $\sin^2 \psi$ law' (first introduced by Macherauch & Müller, 1961), stems from the proportionality of the measured strain to $\sin^2 \psi$ if the P frame of reference has been adopted for the specimen frame of reference (principal state of stress; all stress tensor components σ_{ij}^P are zero for $i \neq j$). A plot of the measured strain *versus* $\sin^2 \psi$ yields a straight line (for constant φ) and the components of the stress tensor can be extracted from the slopes of straight lines for various φ . For stress analysis on the basis of the $\sin^2 \psi$ law [equation (15)] in the presence of shear stresses, *i.e.* the orientation of the P frame of reference is unknown, the reader is referred to §4.

2.5.2. Macroscopically elastically isotropic and anisotropic specimens. In practice, polycrystals composed of elastically isotropic crystallites are seldomly met (tungsten is an example of an elastically isotropic material). In a polycrystal composed of elastically anisotropic crystallites, stresses and strains vary over the (crystallographically) differently oriented crystallites in the specimen, in contrast with a polycrystal composed of elastically isotropic crystallites, where stresses and strains are equal for all differently oriented crystallites. In the presence of this intrinsic elastic anisotropy, the distribution of stresses and strains that occurs is the result of the elastic grain interaction (see Appendix A).

Even if the individual crystallites of a polycrystal are elastically anisotropic, the whole body can still be macroscopically elastically isotropic, which in the following is called quasi-isotropic. This is the case if crystallographic texture does not occur and if the grain interaction is isotropic (*i.e.* direction-dependent grain interaction does not occur). Otherwise, the body is macroscopically elastically anisotropic. These two cases, *i.e.* macroscopic elastic isotropy (quasi-isotropy) and macroscopic elastic anisotropy, have to be considered separately for diffraction stress analysis.

It can be shown by exploiting the symmetries of the elastic properties of subgroups of grains as selected by a diffraction experiment that the concept of diffraction (X-ray) elastic constants (XEC) holds for quasi-isotropic specimens, whereas the concept of diffraction (X-ray) stress factors (XSF) has to be used for elastically anisotropic specimens (Welzel & Mittemeijer, 2003; see also Stickforth, 1966).

In the case of *quasi-isotropic* specimens, a $\sin^2 \psi$ law is obtained, which differs from the $\sin^2 \psi$ law for elastically isotropic specimens [equation (15)] only with respect to the elastic constants S_1 and $\frac{1}{2} S_2$, which have to be replaced by so-

called *hkl*-dependent diffraction (X-ray) elastic constants S_1^{hkl} and $\frac{1}{2}S_2^{hkl}$:

$$\begin{aligned} \varepsilon_{\varphi\psi}^{hkl} &= \{\varepsilon_{33}^L\}_{\varphi\psi}^{hkl} \\ &= \frac{1}{2}S_2^{hkl} \sin^2 \psi [\langle \sigma_{11}^S \rangle \cos^2 \varphi + \langle \sigma_{12}^S \rangle \sin(2\varphi) + \langle \sigma_{22}^S \rangle \sin^2 \varphi] \\ &\quad + \frac{1}{2}S_2^{hkl} [\langle \sigma_{13}^S \rangle \cos \varphi \sin(2\psi) + \langle \sigma_{23}^S \rangle \sin \varphi \sin(2\psi) \\ &\quad + \langle \sigma_{33}^S \rangle \cos^2 \psi] + S_1^{hkl} (\langle \sigma_{11}^S \rangle + \langle \sigma_{22}^S \rangle + \langle \sigma_{33}^S \rangle). \end{aligned} \quad (16)$$

Note that according to the right-hand side of equation (16), in contrast with equation (15), the diffraction strain now depends on the reflection *hkl*. Stresses/strains of individual crystallites are not equal to the corresponding mechanical averages. Thus averaging brackets and averaging braces have to be used.

The modifications of equation (15) necessary to obtain equation (16) were invented on an empirical basis: about ten years after the first strain measurements by means of X-ray diffraction, Möller & Barbers (1935) obtained experimental results indicating that mechanical elastic constants [*i.e.* equation (15)] cannot be used for the stress analysis of polycrystals composed of elastically anisotropic crystallites, *i.e.* diffraction strains differ from mechanical strains due to the intrinsic elastic anisotropy. Diffraction (X-ray) elastic constants were eventually proposed on an empirical basis by Möller & Martin (1939) (see also Bollenrath *et al.*, 1941). For the special cases of the Voigt grain-interaction model (Voigt, 1910) and the Reuss grain-interaction model (Reuss, 1929), it was demonstrated that such XECs can be applied (Möller & Martin, 1939).

At that time, the stress analysis was based on the back-reflection technique involving X-ray sensitive films. The use of

diffractometers for stress analysis and the notion ‘ $\sin^2 \psi$ method’ for an analysis based on equation (16) was established in the 1950s (Macherauch & Müller, 1961; see also Hauk, 1952; Christenson & Rowland, 1953). The analysis was limited to a principal stress state; a generalization to a general stress state was performed by Evenschor & Hauk (1975). A general proof of the validity of equation (16) for any quasi-isotropic polycrystal, independent of the type of grain interaction, was not given until some decades later by Stickforth (1966).

In the case of *macroscopically elastically anisotropic* specimens (*i.e.* in the presence of direction-dependent grain interaction and/or crystallographic texture, *cf.* §5.1), the so-called X-ray stress factors (XSF) have to be employed for diffraction stress analysis (see, for example, Hauk, 1997, and, in particular, Welzel & Mittemeijer, 2003):

$$\{\varepsilon_{33}^L\}_{\varphi\psi}^{hkl} = F_{ij}(\varphi, \psi, hkl) \langle \sigma_{ij}^S \rangle. \quad (17)$$

Experimentally, it was found (for a comprehensive review, see, for example, Hauk, 1997) that non-linear $\sin^2 \psi$ plots are generally observed for textured materials, even for the case of a principal state of stress. Thus, the use of equation (16) for the diffraction stress analysis is not possible, as equation (16) indicates a linear dependence of the diffraction strain on $\sin^2 \psi$ (in the absence of shear stresses).

The pioneering work on the diffraction stress analysis of macroscopically elastically anisotropic specimens was performed by Dölle & Hauk (1978, 1979) for the case of crystallographic texture and by van Leeuwen *et al.* (1999) for the case of direction-dependent grain interaction, and by Leoni *et al.* (2001) for the simultaneous occurrence of direction-dependent grain interaction and crystallographic texture. The theoretical equations that can be used for crystallographically textured polycrystals were originally given, as in the quasi-isotropic case discussed directly above, by an elaboration of a particular model for grain interaction, namely the Reuss model, and in this context the stress factors $F_{kl}(\psi, \varphi, hkl)$ were introduced (Dölle & Hauk, 1978, 1979). A general proof of the validity of equation (17) for any macroscopically elastically anisotropic polycrystal, independent of the type of grain interaction, was given recently by Welzel & Mittemeijer (2003).

Note that $F_{ij}(\psi, \varphi, hkl)$ has no superscript for indicating a reference frame: $F_{ij}(\psi, \varphi, hkl)$ is not a representation of a tensor and thus no reference frame has to be indicated.

The evaluation of the diffraction (X-ray) elastic constants S_1^{hkl} and $\frac{1}{2}S_2^{hkl}$ and the diffraction (X-ray) stress factors $F_{ij}(\psi, \varphi, hkl)$ can be accomplished either by measurement, by applying a known load stress to a specimen under simultaneous lattice strain measurement, or by calculation starting from single-crystal elastic constants by adopting a suitable grain-interaction model (see Appendix A).

A schematic diagram on the use of the two basic formulae, equations (16) and (17), with reference to the structure of the specimen and its elastic properties, is presented in Fig. 3.

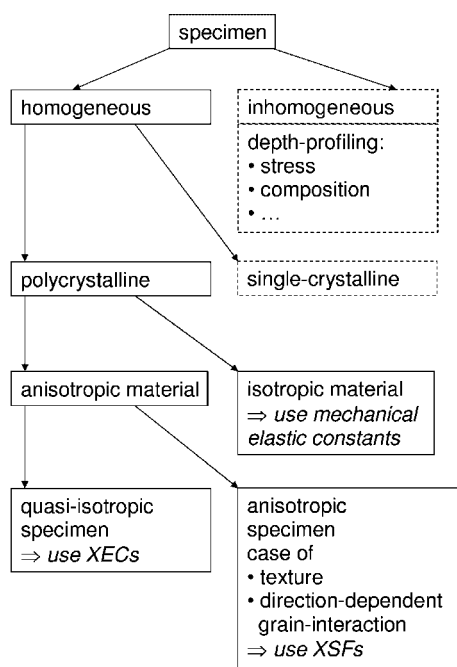


Figure 3 Schematic diagram of different situations in the field of diffraction stress analysis depending on the structure of the specimen and the elastic properties of the material composing the specimen (the cases in dashed boxes are not treated in the present paper).

3. Diffraction geometry

With conventional X-ray diffraction the variation of the angle ψ , defining the measurement direction with respect to the sample surface normal, by tilting the specimen, is accompanied by a variation of the angle of incidence α and thus also of the effective penetration depth of the X-ray beam in the investigated sample. In the case of thin-film analysis, depending on the film thickness and on the X-ray radiation used, the X-rays may penetrate throughout the film into the underlying substrate material. Thus the diffraction peaks of the film and of the substrate can overlap and/or the signal-to-background ratio for diffraction peaks of the film can become very low, both effects hindering the quantitative evaluation of the diffraction profile. Two solutions to this problem have been employed: (i) the diffraction contribution of the substrate using a separate measurement of the uncovered substrate is removed, provided that no changes of the substrate peaks due to the layer deposition occur [apart from absorption (see, for example, Kamminga, Delhez *et al.*, 2000)]; (ii) by keeping the effective penetration depth of the X-ray beam small, the contribution of the substrate is reduced (see, for example, van Acker *et al.*, 1994).

The dependence of the beam penetration, as expressed by the information depth [for definitions of various measures of information depth, see Delhez *et al.* (1987)], on the angle of incidence is utilized by dedicated methods (grazing-incidence method and scattering vector method; see §3.2) to analyse the stress at a fixed depth and thus to allow the determination of stress profiles in films or near-surface regions of bulk materials.

A measure for the average information depth (for an 'infinitely' thick sample) is the so-called $1/e$ penetration depth, τ . It is the centre of gravity of the distribution of measured diffracted intensity *versus* depth; about 63% of the diffracted intensity originates from a volume confined by depth τ below the sample surface. τ is given by

$$\tau = \sin \alpha \sin \beta / \mu(\sin \alpha + \sin \beta), \quad (18)$$

where α and β denote the angle of incidence and exit, respectively, of the X-ray beam with respect to the sample surface, and μ is the effective linear absorption coefficient of the material depending on the radiation used.

First, measurement methods which do not take care of the variation of the penetration depth during the measurement are discussed in §3.1. §3.2 focuses on grazing-incidence methods, where the penetration depth can be controlled by a proper choice of the instrumental angles.

3.1. Conventional X-ray diffraction

With the conventional diffraction geometry, no measures are taken to control the penetration depth of the X-rays in the sample by a defined angle of incidence, α , and/or of exit, β . The rotation angles of the instrument are used only to bring $\{hkl\}$ planes, which are oriented in a certain way in the sample, into diffraction condition, *i.e.* to align the normal of the $\{hkl\}$ planes parallel to the diffraction vector (L_3 axis of the laboratory system L; see Fig. 2).

In the following, the different angles required for the description of diffraction geometries are defined. The angles φ and ψ , describing the orientation of the normal of $\{hkl\}$ planes with respect to the specimen system S (see §2, Fig. 2) in the $\sin^2 \psi$ formulae [see equations (16) and (17)] and the rotation angles ϕ , ω and χ of the instrument, describing the orientation of the sample with respect to the laboratory system L (see Fig. 4), have to be distinguished.

The instrumental angles are as follows.

2θ = diffraction angle, set by the detector position. In the following the angle θ is strictly used as the Bragg angle (half of the diffraction angle, *i.e.* angle between the incident beam and crystallographic planes in diffraction condition) and not as the angle between the incident beam and the sample surface.

ϕ = rotation around the normal of the plate of the sample stage. Usually the sample is mounted on the stage such that the ϕ axis and the φ axis are parallel and the two rotation angles are then simply related by a constant (rotational) offset.

ω = angle of rotation of the sample around an axis perpendicular to the diffraction plane, *i.e.* parallel to the 2θ axis and perpendicular to the χ axis. For symmetric diffraction

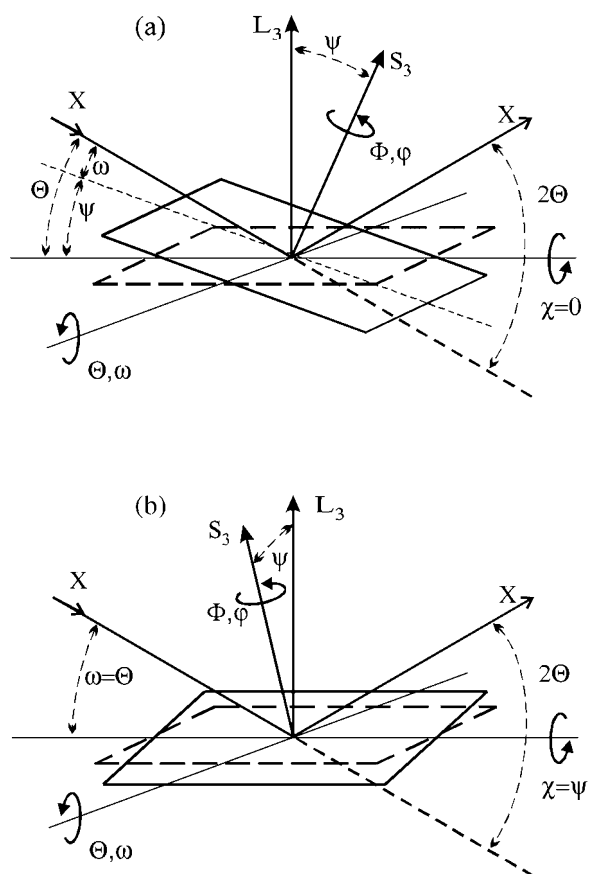


Figure 4
Definition of the various angles required to describe the diffraction geometries and variation of the angle ψ using (a) the ω mode (shown for $\psi < 0$) or (b) the χ mode. L_3 is the diffraction vector, S_3 is the surface normal.

(Bragg–Brentano) condition: $\omega = \theta$ and (in addition) for $\chi = 0$: $\alpha = \omega$.

χ = angle of rotation of the sample around an axis defined by the intersection of the diffraction plane and the sample surface (plate of the sample stage), *i.e.* perpendicular to the ω axis and the 2θ axis.

Confusion can be (but often is not) avoided if the angles ω and χ are not intermixed with the angles θ and ψ , respectively (note that the term ‘ $2\theta/\theta$ scan’ is misleading and it should be replaced by the term ‘ $2\theta/\omega$ scan’).

Diffraction planes $\{hkl\}$ with a specific orientation φ and ψ in the specimen system S can be selected by setting of the instrumental angles 2θ , ϕ , ω and χ . The possibility to set an angle ψ either by ω or by χ (or a combination of both) leads to the distinction between the ω mode and the χ mode in a stress measurement (where the scan over the diffraction peak at fixed ψ is in both cases performed by a $2\theta/\omega$ scan).

3.1.1. ω mode, $\chi = 0$ (Fig. 4a). Variation of ω [at fixed $\theta = \theta^{hkl}$, *cf.* equation (2)] provides a variation of the inclination ψ of the measured $\{hkl\}$ planes with respect to the sample normal according to $\psi = \omega - \theta$ (the opposite convention $\psi = \theta - \omega$ is also found in the literature; however, note that, if the polar angles φ and ψ are defined to specify the measuring direction in the sample coordinate system, ψ is always positive). Because of $\chi = 0$, the angle α of incidence is directly given by the angle ω ; the exit angle is $\beta = 2\theta - \omega = \theta - \psi$. With the ω mode only a restricted range of $|\psi| < \theta$ is accessible (the limit is given by the position where the incident or the diffracted beam is parallel to the sample surface).

Inserting $\alpha = \theta + \psi$ and $\beta = \theta - \psi$ into equation (18), the penetration depth in terms of the two angles θ and ψ is obtained:

$$\tau_{\omega} = \frac{\sin^2 \theta - \sin^2 \psi}{2 \mu \sin \theta \cos \psi} \quad (\psi = \omega - \theta). \quad (19)$$

3.1.2. χ mode (ψ mode), $\omega = \theta$ (Fig. 4b). For χ mode, the angle χ is the same as the angle ψ (therefore it is often also called ψ mode; another name is side-inclination method). Variation of χ (at fixed $\theta = \theta^{hkl}$) provides a variation of the inclination ψ of the measured $\{hkl\}$ planes with respect to the sample normal. The true angle α of incidence (equal to the angle of exit β) is given by

$$\sin \alpha (= \sin \beta) = \sin \omega \cos \chi. \quad (20)$$

From equations (18) and (20) the penetration depth in terms of the two angles θ and ψ is obtained:

$$\tau_{\chi} = \frac{\sin \theta}{2 \mu} \cos \psi \quad (\psi = \chi). \quad (21)$$

Note that the rotation angle φ describing the measurement direction within the plane of the sample differs by 90° for the χ and ω modes.

The errors in measured peak positions $2\theta^{hkl}$ due to non-ideal beam optics and to misalignment are different for the χ mode and the ω mode. In particular, with the ω mode the defocusing error is different for positive ($\omega > \theta$) and negative

($\omega < \theta$) tilts of the sample. For corrections for non-ideal beam optics, see Noyan & Cohen (1987) (and references therein) and Vermeulen & Houtman (2000).

3.1.3. Combined ω/χ mode. For a tilt of the sample around both the ω axis and the χ axis simultaneously, the values of the various angles are not obvious but can be calculated by expressing the directions of the incoming beam, the diffracted beam and the diffraction vector in the S system, employing appropriate rotation matrices. The measuring direction (φ , ψ) in the S system is given by

$$\varphi = \phi + \arctan \left[\frac{-\sin \chi}{\tan(\omega - \theta)} \right] \quad (22)$$

and

$$\psi = \frac{\omega - \theta}{|\omega - \theta|} \arccos[\cos \chi \cos(\omega - \theta)]. \quad (23)$$

The angle of incidence, α , is given by equation (20) and the exit angle of the diffracted beam with respect to the sample surface, β , is given by

$$\sin \beta = \sin(2\theta - \omega) \cos \chi. \quad (24)$$

With conventional X-ray diffraction, whatever the mode considered, all combinations of the instrumental angles ϕ , ω , χ and θ are possible, because the orientation of the specimen and the diffraction angle θ can be chosen independently (in contrast to the grazing-incidence methods; see below). However, the choice of the reference position of the sample (*i.e.* the choice of the orientation of the ψ axis, ω or χ mode, and the direction $\varphi = 0^\circ$ with respect to the sample geometry) defines the frame of reference for the tensor components (ε_{ij}^S) and (σ_{ij}^S).

3.2. Grazing-incidence X-ray diffraction

For very thin surface-adjacent layers, the X-ray diffraction measurement of specimen properties, like residual stress and crystallite orientation distribution, is possible by using small angles of incidence [introduced as the low incident-beam angle diffraction method (LIBAD) by van Acker *et al.* (1994)]. The grazing-incidence X-ray diffraction (GIXD) method (using so-called in-plane diffraction geometry where the diffraction vector is parallel to the sample surface) was originally developed by Marra *et al.* (1979). Using small angles α of incidence the effective sampling volume is confined to a relatively small volume adjacent to the surface of the sample yielding higher diffracted intensities from this volume than with conventional X-ray diffraction methods. Sometimes in the literature the terms ‘grazing-incidence XRD’ and ‘glancing-incidence XRD’ are used (see, for example, Noyan *et al.*, 1995) to distinguish, respectively, between angles α of incidence very close to the critical angle for total external reflection (some tenths of a degree), where the penetration depth is of the order of a few nanometres only, and angles α of incidence of a few degrees, where the penetration depth is of the order of a few micrometres. Examples are shown in Fig. 5. In the following the term grazing-incidence X-ray diffraction

(GIXD) is used for geometries involving both (overlapping) ranges of angles of incidence mentioned above.

The GIXD method for stress analysis is useful in two cases: (i) to restrict the effective penetration depth to a defined small value when the stress state at (close to) the surface of a body has to be determined or when stress analyses have to be performed for very thin films for which problems of overlap with substrate peaks can occur; (ii) to determine stress gradients from diffraction measurements at different effective penetration depths by varying the angle α of incidence or the wavelength. If the angle α of incidence is not too close to the critical angle for total reflection and small compared with the exit angle β (i.e. for θ^{hkl} not in the vicinity of 0 or 90° in the case of the ω mode), the effective penetration depth is approximated by $\tau = \sin\alpha/\mu$ [cf. equation (18)]. In the vicinity of the critical angle, equation (18) no longer holds and τ varies more strongly with α than according to equation (18) (see Fig. 5). Note that during the variation of the angle of incidence α to change the X-ray penetration depth, the angle ψ remains nearly constant [see equation (25) below].

The refraction of the incident and the diffracted X-ray beam at the surface of the sample causes a shift $\Delta 2\theta^{hkl}$ of the measured peak position to larger angles with respect to the theoretical Bragg angle $2\theta^{hkl}$, which has to be corrected for, in particular in the range of small angles of incidence α (see, for example, Toney & Brennan, 1989; Dümmer *et al.*, 1999). For angles of incidence close to the critical angle for total reflection, the shift $\Delta 2\theta^{hkl}$ can attain values of some tenths of a degree with reference to the critical angle for total reflection; the shift $\Delta 2\theta^{hkl}$ decreases with increasing α approximately according to $1/\alpha$ down to small values, typically of the order of 10^{-3} degrees.

The task of a GIXD stress measurement is to measure the strain, ϵ_{ψ}^{hkl} , at different angles ψ under the constraint of a small and fixed value of the penetration depth τ . As the instrumental angle ω has to be used for setting a fixed angle of incidence α , it cannot be used for the variation of ψ . This represents a loss of freedom in comparison with conventional

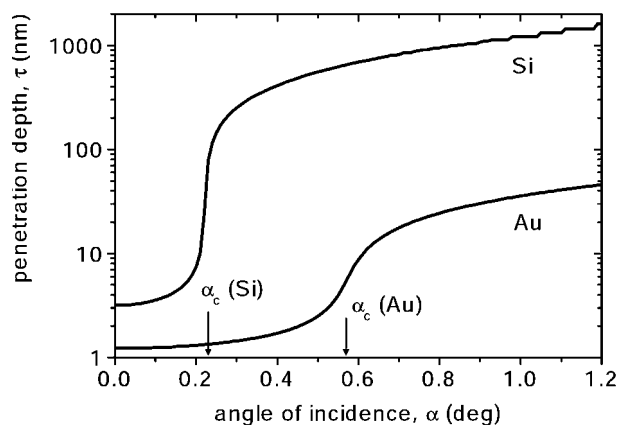


Figure 5
Penetration depth, τ ($1/e$ definition), for Cu $K\alpha$ radiation in Si and Au versus the angle of incidence, α , of the X-ray beam calculated according to Parrat (1954). In the vicinity of the critical angle, α_c , for total reflection, a strong variation of τ occurs.

XRD. Depending on the specific diffraction geometry, the range of accessible ψ angles is restricted (see below). In the case of a textured film, the available range may not cover (all) the ψ angles at which diffraction peaks of the specimen occur. For the rotation angle φ , no constraints owing to the condition of grazing incidence exist.

3.2.1. Methods for the variation of the angle ψ . In GIXD, in principle, three methods to achieve a variation of ψ are possible (two of them are illustrated in Fig. 6).

(i) *Multiple χ .* For one family of $\{hkl\}$ planes, measurements at different χ angles are performed in the same way as with the conventional χ mode, i.e. the angle χ is used to vary the angle ψ . In addition, a small incidence angle α is chosen by ω ($= \alpha$ at $\chi = 0$). Thus this method is a combination of the χ mode and the ω mode (because of the non-symmetrical setting, $\omega \neq \theta$: $\psi \neq \chi$). To keep the angle α constant, for each $\chi \neq 0$ the angle ω has to be adjusted according to equation (20). Note that to keep the angle φ fixed (for the measurement of a stress state which is not rotationally symmetric) the instrumental angle ϕ also has to be varied properly. Multiple- χ GIXD has been

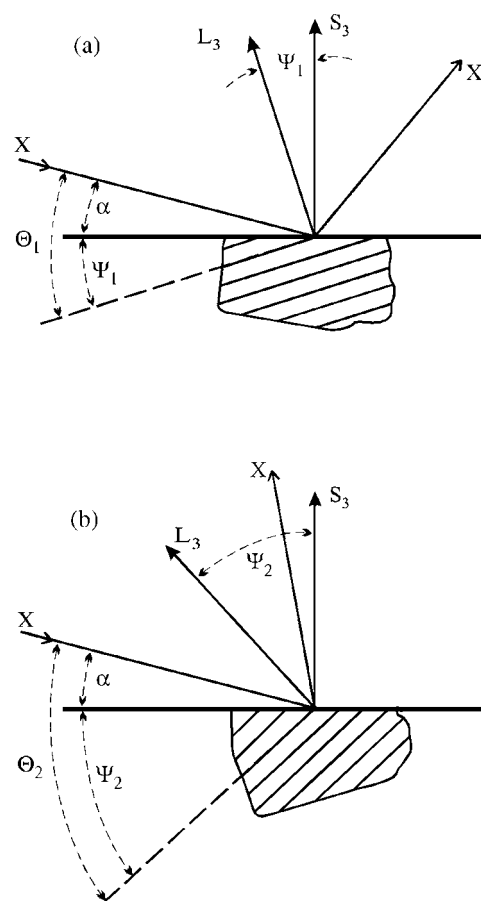


Figure 6
Grazing-incidence diffraction, multiple hkl and multiple wavelengths: Illustration of the variation of the angle $\psi = |\theta^{hkl} - \alpha|$ by measurements at different Bragg angles θ^{hkl} , θ_1 (a) and θ_2 (b), using either two different hkl or two different wavelengths (in the latter case α has to be adjusted to keep τ fixed). The axis L_3 is the diffraction vector, axis S_3 is the surface normal (see also Fig. 4); the incident and diffracted X-ray beams are indicated by X.

applied to a ZrN film on Si(100) and to a TiN film on steel by Ma *et al.* (2002). There also the rotation matrix describing the spatial relation between the laboratory (L) system and the sample (S) system for this diffraction geometry is given.

(ii) *Multiple {hkl}*. During the measurement, the incidence angle ($\alpha = \omega$ at $\chi = 0$) is fixed and several *hkl* diffraction lines are recorded by 2θ scans (Fig. 6). The inclination angle ψ for a set of $\{hkl\}$ planes is given by

$$\psi = \theta^{hkl} - \alpha, \quad (25)$$

where θ^{hkl} is the Bragg angle. For small and constant α , the path of the reflected beam in the sample is small compared with that of the incoming beam and thus the penetration depth remains nearly constant for different values of $2\theta^{hkl}$, *i.e.* for different $\{hkl\}$ diffraction planes (van Acker *et al.*, 1994). In contrast to conventional X-ray diffraction, where the angles ψ and θ can be chosen independently, with GIXD the dependence between the angles ψ and θ^{hkl} , for given α [equation (25)], places a constraint on the possible measuring combinations (only one degree of freedom remains). The multiple- $\{hkl\}$ GIXD method has been applied to *e.g.* TiN coatings on steel by Quaeys *et al.* (1996) and TiN coatings on WC by Skrzypek & Baczmanski (2001) and Skrzypek *et al.* (2001).

(iii) *Multiple wavelengths*. Measurements for one family of $\{hkl\}$ planes using different wavelengths, *i.e.* different Bragg angles θ^{hkl} , correspond to different angles ψ [equation (25), Fig. 6]. For each wavelength, the incidence angle α has to be adjusted to keep the depth τ (depending on the absorption coefficient μ) constant. With this method a lattice strain plot *versus* $\sin^2\psi$ can be obtained in the same way as with the conventional $\sin^2\psi$ method (§4). The multiple-wavelength GIXD method has been applied by Predecki *et al.* (1993) to determine the residual strain in an Al film on Si.

3.2.2. Scattering vector method. A special method dedicated to the measurement of stress depth profiles ($\langle\sigma_{ij}^S(\tau)\rangle$), the so-called scattering vector method, was developed by Genzel (1997, and references therein). During a rotation of the specimen around the diffraction vector (L_3 axis in Fig. 2), by an angle η , the measurement direction with respect to the specimen, defined by the angles φ and ψ , remains unchanged. It is possible to vary the angle η by appropriate simultaneous variations of the instrumental angles ϕ , ω and χ (thus the scattering vector method consists of a combination of the ω and the χ modes). This is accompanied by a variation of the angles of incidence and of exit, α and β (if $\psi > 0$), and thus allows diffraction measurements for different depths τ [see equation (18)] as a function of η . A general formulation for the $1/e$ penetration depth τ is given by (Genzel, 1994)

$$\tau = \frac{\sin^2\theta - \sin^2\psi + \cos^2\theta \sin^2\psi \sin^2\eta}{2\mu \sin\theta \cos\psi}. \quad (26)$$

For $\psi \leq \theta^{hkl}$ the τ range covered with an η scan from 0 to 90° is limited by the values of the penetration depths of the ω and χ modes: $\tau(\eta = 0^\circ) = \tau_\omega$ [equation (19)] and $\tau(\eta = 90^\circ) = \tau_\chi$ [equation (21)]. For $\psi > \theta^{hkl}$, the range of η from η_{\min} to 90° is possible, where η_{\min} is given by $\tau = 0$ in equation (26), corresponding to an angle of incidence of zero.

Performing depth profiling by an η scan at fixed (φ, ψ) and repeating this at different (φ, ψ) yields a set of $d_{\varphi\psi}^{hkl}[\tau(\eta)]$ profiles, from which the individual components $\sigma_{ij}(\tau)$ of the macroscopic stress tensor can be derived using one of the stress analysis methods (see §4). For practical examples of the evaluation of stress depth profiles using the scattering vector method, see Genzel (1999) and Genzel *et al.* (1999).

3.2.3. Depth profiling. In principle, all GIXD methods described above can be employed for the determination of stress profiles along the direction $z = S_3$ perpendicular to the sample surface. The relevant components of the stress tensor $\sigma_{ij}(\tau)$ have to be determined in dependence of the X-ray penetration depth τ . This requires the determination of $\varepsilon_{\varphi\psi}^{hkl}$ at different angles ψ (and φ) as a function of the penetration depth τ . The profile $\sigma_{ij}(\tau)$, thus obtained from the measurements, and the corresponding profile $\sigma_{ij}(z)$ are related by (Dölle, 1979)

$$\sigma_{ij}(\tau) = \int_0^t \sigma_{ij}(z) \exp(-z/\tau) dz \bigg/ \int_0^t \exp(-z/\tau) dz, \quad (27)$$

where t is the thickness of the sample.

Different procedures for the inversion of equation (27), *i.e.* calculating $\sigma_{ij}(z)$ from $\sigma_{ij}(\tau)$, were proposed in the literature, such as the use of inverse Laplace transforms [for an example, see Predecki *et al.* (1993) where also problems and the uniqueness of the results are discussed], or least-squares fitting using model functions for the profile $\sigma_{ij}(z)$ (Eigenmann *et al.*, 1992; Leverenz *et al.*, 1996; Behnken & Hauk, 2000).

4. Macroscopically elastically isotropic specimens

In this section, stress analysis methods for macroscopically elastically isotropic specimens are discussed. The underlying equation for all these methods is equation (16) (the traditional ‘ $\sin^2\psi$ law’), relating the lattice strain $\varepsilon_{\varphi\psi}^{hkl}$ in a certain measurement direction (φ, ψ) to the components of the mechanical stress tensor (expressed in the specimen frame of reference S) for a macroscopically elastically isotropic specimen. In the case of homogeneous stress states considered here, a maximum of six independent stress tensor components are to be determined because the stress tensor, comprising nine components, is symmetric (*i.e.* $\langle\sigma_{ij}\rangle = \langle\sigma_{ji}\rangle$). To this end, lattice strains are to be measured for at least as many (suitable) different directions as there are unknown stress tensor components. Two degrees of freedom for the variation of the direction of the lattice strain measurement exist: the angles φ and ψ , defining the orientation of the diffraction vector with respect to the specimen frame of reference (see Fig. 1).

The determination of the unknown stress tensor components from a number of lattice strain measurements is equivalent to the solution of a system of linear equations where the independent stress tensor components are the basic unknowns. Additional unknowns, for example the stress-free lattice constants (provided that the stress state is not triaxial; see below and, in particular, §4.4), may also be determined by a diffraction stress analysis. In general, the number of

measured lattice strains is large compared with the number of unknowns, and some kind of fitting is then employed.

Most of the methods described in this section have been designed for practical purposes in such a way that the traditional ‘ $\sin^2\psi$ law’ [equation (16)] is rearranged (and, depending on the number of stress tensor components to be determined, simplified) in order to obtain linear plots of lattice strain *versus* certain functions of φ , ψ and hkl (see below). The stress tensor components are determined from the slopes and intercepts of the corresponding straight lines as obtained by linear regression. Thus ‘complicated’ fitting procedures (of course generally possible in all cases) are avoided. A common example is the well known $\sin^2\psi$ method applied to a plane rotationally symmetric state of stress, where the slope of the straight line [divided by the diffraction (X-ray) elastic constant $\frac{1}{2}S_2^{hkl}$], obtained by linear regression in a plot of the lattice strain *versus* $\sin^2\psi$, yields the stress.

The methods of analysis can be classified in different ways, for example according to the angle, φ or ψ , preferred for a variation of the measurement direction [‘ ψ method(s)’ and ‘ φ method(s)’], according to the number of stress tensor components which can be determined using a particular method, or according to the number of hkl reflections used simultaneously in the analysis.

In §4.1, methods are described which employ lattice strains measured using one particular hkl reflection, whereas §4.2 presents methods capable of deducing stress from lattice strains measured employing multiple hkl reflections simultaneously. The different methods have both advantages and disadvantages in terms of their susceptibility to measurement errors. Some of the methods allow diffraction stress analysis at a fixed penetration depth, making them especially suitable for the analysis of stress profiles. Comparative comments on the different methods are given in §4.4. For the calculation of the diffraction (X-ray) elastic constants, the reader is referred to Appendix A.

4.1. Single hkl reflection

4.1.1. $\sin^2\psi$ – $\sin(2\psi)$ method: analysis of a triaxial stress state. The general strain–stress relation, equation (16), can be rewritten as

$$\varepsilon_{\varphi\psi}^{hkl} = \frac{1}{2}S_2^{hkl} [(\langle\sigma_{\varphi}^S\rangle - \langle\sigma_{33}^S\rangle) \sin^2\psi + \langle\tau_{\varphi}^S\rangle \sin(2\psi)] + \varepsilon_{\varphi 0^\circ}^{hkl} \quad (28)$$

using the abbreviations $\langle\sigma_{\varphi}^S\rangle$, $\langle\tau_{\varphi}^S\rangle$ and $\varepsilon_{\varphi 0^\circ}^{hkl}$:

$$\langle\sigma_{\varphi}^S\rangle = \langle\sigma_{11}^S\rangle \cos^2\varphi + \langle\sigma_{12}^S\rangle \sin(2\varphi) + \langle\sigma_{22}^S\rangle \sin^2\varphi, \quad (29)$$

$$\langle\tau_{\varphi}^S\rangle = \langle\sigma_{13}^S\rangle \cos\varphi + \langle\sigma_{23}^S\rangle \sin\varphi \quad (30)$$

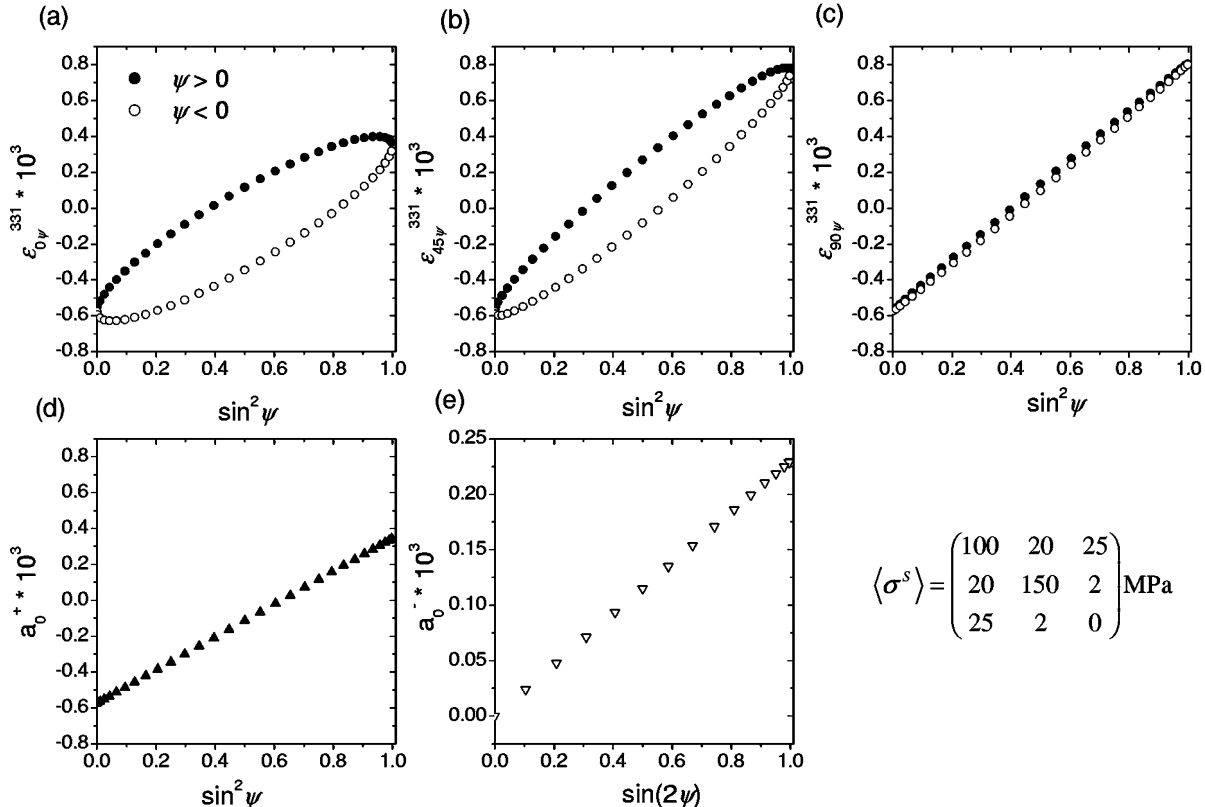


Figure 7

Stress analysis employing the $\sin^2\psi$ – $\sin(2\psi)$ method: calculated example. Lattice strain for the 331 reflection of a macroscopically elastically isotropic copper specimen subjected to the stress state given by the mechanical stress tensor in the figure: (a) at $\varphi = 0^\circ$, (b) at $\varphi = 45^\circ$ and (c) at $\varphi = 90^\circ$ (filled circles for positive tilt, open circles for negative tilt). The components of the stress tensor can be obtained on the basis of plots of a_φ^+ *versus* $\sin^2\psi$ (d) and a_φ^- *versus* $\sin(2\psi)$ (e) (shown for $\varphi = 0^\circ$). For details, see text.

and

$$\varepsilon_{\varphi 0^\circ}^{hkl} = \frac{1}{2} S_2^{hkl} \langle \sigma_{33}^S \rangle + S_1^{hkl} (\langle \sigma_{11}^S \rangle + \langle \sigma_{22}^S \rangle + \langle \sigma_{33}^S \rangle). \quad (31)$$

For the determination of the off-diagonal stress tensor components, a procedure suggested by Dölle & Hauk (1976) can be employed (see also Evenschor & Hauk, 1975). An example of a stress analysis on the basis of this method is shown in Fig. 7.

For a general stress state, the lattice strain $\varepsilon_{\varphi\psi}^{hkl}$ is neither a linear function of $\sin^2\psi$ nor a linear function of $\sin(2\psi)$. The parameters a_φ^+ and a_φ^- are obtained from the lattice strains $\varepsilon_{\varphi\psi>0}^{hkl}$ and $\varepsilon_{\varphi\psi<0}^{hkl}$ for a given φ , at fixed $|\psi|$, i.e. by using lattice strain measurements at positive and negative values of the angle ψ , respectively:

$$a_\varphi^+ = \frac{1}{2} (\varepsilon_{\varphi\psi>0}^{hkl} + \varepsilon_{\varphi\psi<0}^{hkl}) = \frac{1}{2} S_2^{hkl} (\langle \sigma_\varphi^S \rangle - \langle \sigma_{33}^S \rangle) \sin^2\psi + \varepsilon_{\varphi 0^\circ}^{hkl} \quad (32)$$

and

$$a_\varphi^- = \frac{1}{2} (\varepsilon_{\varphi\psi>0}^{hkl} - \varepsilon_{\varphi\psi<0}^{hkl}) = \frac{1}{2} S_2^{hkl} \langle \tau_\varphi^S \rangle \sin(2\psi). \quad (33)$$

Linear relations are now obtained for a_φ^+ (when plotted *versus* $\sin^2\psi$) and a_φ^- [when plotted *versus* $\sin(2\psi)$]. Note that by introducing a_φ^+ and a_φ^- , the shear components $\langle \sigma_{13}^S \rangle$ and $\langle \sigma_{23}^S \rangle$ are treated independently from the other components of the stress tensor. The lattice strain is measured at three rotation angles $\varphi = 0, 90$ and 45° for several pairs of positive and negative values of the angle ψ . Then, a plot of the data for a_φ^+ *versus* $\sin^2\psi$ leads to a straight line (Fig. 7). The slope A_φ^+ can be written as [cf. equations (29) and (32)]:

$$A_\varphi^+ = \frac{1}{2} S_2^{hkl} \left[\frac{\langle \sigma_{11}^S \rangle + \langle \sigma_{22}^S \rangle}{2} + \frac{\langle \sigma_{11}^S \rangle - \langle \sigma_{22}^S \rangle}{2} \cos(2\varphi) + \langle \sigma_{12}^S \rangle \sin(2\varphi) - \langle \sigma_{33}^S \rangle \right]. \quad (34)$$

The slopes at the specific φ angles, $A_{0^\circ}^+$, $A_{90^\circ}^+$ and $A_{45^\circ}^+$, present three equations for the four unknown stress components $\langle \sigma_{11}^S \rangle$, $\langle \sigma_{22}^S \rangle$, $\langle \sigma_{33}^S \rangle$ and $\langle \sigma_{12}^S \rangle$.

The component $\langle \sigma_{12}^S \rangle$ can be directly calculated from

$$\langle \sigma_{12}^S \rangle = \frac{1}{\frac{1}{2} S_2^{hkl}} \left(A_{45^\circ}^+ - \frac{A_{0^\circ}^+ + A_{90^\circ}^+}{2} \right). \quad (35)$$

For the other three unknown components, an additional equation is needed, which is provided by equation (31). The lattice strain $\varepsilon_{\varphi 0^\circ}^{hkl}$ is measured at $\psi = 0^\circ$ (it is advised to determine an average of measurements at several φ angles). From equation (31) and from the quantities $A_{0^\circ}^+$ and $A_{90^\circ}^+$ [equation (34)] it follows that

$$\langle \sigma_{33}^S \rangle = \frac{1}{\frac{1}{2} S_2^{hkl} + 3 S_1^{hkl}} \left[\varepsilon_{\varphi 0^\circ}^{hkl} - \frac{S_1^{hkl}}{\frac{1}{2} S_2^{hkl}} (A_{0^\circ}^+ + A_{90^\circ}^+) \right], \quad (36)$$

$$\langle \sigma_{11}^S \rangle = \frac{A_{0^\circ}^+}{\frac{1}{2} S_2^{hkl}} + \langle \sigma_{33}^S \rangle \quad (37)$$

and

$$\langle \sigma_{22}^S \rangle = \frac{A_{90^\circ}^+}{\frac{1}{2} S_2^{hkl}} + \langle \sigma_{33}^S \rangle. \quad (38)$$

The shear stress components $\langle \sigma_{13}^S \rangle$ and $\langle \sigma_{23}^S \rangle$ are derived from $\langle \tau_\varphi^S \rangle$ [equation (30)] as follows.

Plots of a_φ^- for $\varphi = 0$ and 90° (Fig. 7) *versus* $\sin(2\psi)$ lead to straight lines (with offset = 0) with slopes $A_{0^\circ}^-$ and $A_{90^\circ}^-$, respectively. The shear components $\langle \sigma_{13}^S \rangle$ and $\langle \sigma_{23}^S \rangle$ are obtained from

$$\langle \sigma_{13}^S \rangle = \frac{A_{0^\circ}^-}{\frac{1}{2} S_2^{hkl}} \quad (39)$$

and

$$\langle \sigma_{23}^S \rangle = \frac{A_{90^\circ}^-}{\frac{1}{2} S_2^{hkl}}. \quad (40)$$

It should be mentioned that two situations occurring frequently in practice, which can be handled by the above-described method, are: (i) triaxial with $\langle \sigma_{33}^S \rangle = 0$, but $\langle \sigma_{3i}^S \rangle = \langle \sigma_{3i}^S \rangle \neq 0$ for $i = 1, 2$; note that in this case, knowledge of the absolute strain at $\psi = 0^\circ$, $\varepsilon_{\varphi 0^\circ}^{hkl}$, is not required, cf. equation (36); (ii) triaxial with $\langle \sigma_{33}^S \rangle = 0$, but $\langle \sigma_{3i}^S \rangle = \langle \sigma_{3i}^S \rangle \neq 0$ for $i = 1, 2$ and principal axes known with respect to the in-plane directions (i.e. $\langle \sigma_{12}^S \rangle = 0$); note that in this case, knowledge of the absolute strain at $\psi = 0^\circ$, $\varepsilon_{\varphi 0^\circ}^{hkl}$, is not required, cf. equation (36), and measurements at $\varphi = 45^\circ$ are not necessary, cf. equation (35).

The general method described above can be considerably simplified when the number of non-zero stress tensor components is reduced. The following simplifications with respect to the general triaxial case (six unknown non-zero stress tensor components) can be considered.

- (i) Triaxial with principal axes known (three non-zero stress tensor components).
- (ii) Biaxial with principal axes unknown (three non-zero stress tensor components).
- (iii) Biaxial with principal axes known (two non-zero stress tensor components).
- (iv) Biaxial, rotationally symmetric (one independent non-zero stress tensor component).
- (v) Uniaxial (one independent non-zero stress tensor component).

In the following, these methods are referred to as variants of the $\sin^2\psi$ method because in these cases, plots of lattice strain *versus* $\sin^2\psi$ suffice for stress analysis and no special quantities as in the case of a triaxial stress state (like a_φ^+ ; see above) have to be considered.

4.1.2. $\sin^2\psi$ method: analysis of a triaxial principal stress state. For a triaxial principal state of stress, the unknown stress tensor components are $\langle \sigma_{11}^S \rangle (= \langle \sigma_{11}^P \rangle)$, $\langle \sigma_{22}^S \rangle (= \langle \sigma_{22}^P \rangle)$ and $\langle \sigma_{33}^S \rangle (= \langle \sigma_{33}^P \rangle)$. The strain–stress relation, equation (16), simplifies to

$$\varepsilon_{\varphi\psi}^{hkl} = \frac{1}{2} S_2^{hkl} (\cos^2\varphi \langle \sigma_{11}^S \rangle + \sin^2\varphi \langle \sigma_{22}^S \rangle - \langle \sigma_{33}^S \rangle) \sin^2\psi + S_1^{hkl} (\langle \sigma_{11}^S \rangle + \langle \sigma_{22}^S \rangle + \langle \sigma_{33}^S \rangle) + \frac{1}{2} S_2^{hkl} \langle \sigma_{33}^S \rangle. \quad (41)$$

For $\varphi = 0^\circ$, equation (41) reads:

$$\begin{aligned} \varepsilon_{0^\circ\psi}^{hkl} = & \frac{1}{2} S_2^{hkl} (\langle \sigma_{11}^S \rangle - \langle \sigma_{33}^S \rangle) \sin^2 \psi \\ & + S_1^{hkl} (\langle \sigma_{11}^S \rangle + \langle \sigma_{22}^S \rangle + \langle \sigma_{33}^S \rangle) + \frac{1}{2} S_2^{hkl} \langle \sigma_{33}^S \rangle. \end{aligned} \quad (42)$$

For $\varphi = 90^\circ$:

$$\begin{aligned} \varepsilon_{90^\circ\psi}^{hkl} = & \frac{1}{2} S_2^{hkl} (\langle \sigma_{22}^S \rangle - \langle \sigma_{33}^S \rangle) \sin^2 \psi \\ & + S_1^{hkl} (\langle \sigma_{11}^S \rangle + \langle \sigma_{22}^S \rangle + \langle \sigma_{33}^S \rangle) + \frac{1}{2} S_2^{hkl} \langle \sigma_{33}^S \rangle. \end{aligned} \quad (43)$$

For $\psi = 0^\circ$:

$$\varepsilon_{\varphi 0^\circ}^{hkl} = S_1^{hkl} (\langle \sigma_{11}^S \rangle + \langle \sigma_{22}^S \rangle + \langle \sigma_{33}^S \rangle) + \frac{1}{2} S_2^{hkl} \langle \sigma_{33}^S \rangle. \quad (44)$$

The lattice strain is measured at two rotation angles $\varphi = 0$ and 90° for a fixed hkl reflection at several tilt angles ψ (*cf.* Hauk, 1997). The slopes, A_{0° and A_{90° , taken from the straight lines obtained in plots of $\varepsilon_{0^\circ\psi}^{hkl}$ and $\varepsilon_{90^\circ\psi}^{hkl}$, respectively, *versus* $\sin^2 \psi$ [equations (42) and (43)] present two equations for the stresses $\langle \sigma_{11}^S \rangle$, $\langle \sigma_{22}^S \rangle$ and $\langle \sigma_{33}^S \rangle$. The third equation for the determination of the three stress components is obtained from $\varepsilon_{\varphi 0^\circ}^{hkl}$, *i.e.* a measurement at $\psi = 0^\circ$, equation (44) (where in practice an average over measurements at several φ angles is recommended).

Solving the three equations for the three (principal) stress components gives:

$$\langle \sigma_{33}^S \rangle = \frac{1}{\frac{1}{2} S_2^{hkl} + 3 S_1^{hkl}} \left[\varepsilon_{\varphi 0^\circ}^{hkl} - \frac{S_1^{hkl}}{\frac{1}{2} S_2^{hkl}} (A_{0^\circ} + A_{90^\circ}) \right], \quad (45)$$

$$\langle \sigma_{11}^S \rangle = \frac{A_{0^\circ}}{\frac{1}{2} S_2^{hkl}} + \langle \sigma_{33}^S \rangle \quad (46)$$

and

$$\langle \sigma_{22}^S \rangle = \frac{A_{90^\circ}}{\frac{1}{2} S_2^{hkl}} + \langle \sigma_{33}^S \rangle. \quad (47)$$

4.1.3. $\sin^2 \psi$ method: analysis of a biaxial stress state. For a plane state of stress, where the two principal axes are unknown (but in the plane of the surface of the specimen), the occurring stress components are $\langle \sigma_{11}^S \rangle$, $\langle \sigma_{22}^S \rangle$ and $\langle \sigma_{12}^S \rangle$ (stress perpendicular to the surface, $\langle \sigma_{33}^S \rangle$, is zero) and thus equation (16) becomes

$$\begin{aligned} \varepsilon_{\varphi\psi}^{hkl} = & \frac{1}{2} S_2^{hkl} [\cos^2 \varphi \langle \sigma_{11}^S \rangle + \sin(2\varphi) \langle \sigma_{12}^S \rangle + \sin^2 \varphi \langle \sigma_{22}^S \rangle] \sin^2 \psi \\ & + S_1^{hkl} (\langle \sigma_{11}^S \rangle + \langle \sigma_{22}^S \rangle). \end{aligned} \quad (48)$$

For $\varphi = 0^\circ$, equation (48) reads:

$$\varepsilon_{0^\circ\psi}^{hkl} = \frac{1}{2} S_2^{hkl} \langle \sigma_{11}^S \rangle \sin^2 \psi + S_1^{hkl} (\langle \sigma_{11}^S \rangle + \langle \sigma_{22}^S \rangle). \quad (49)$$

For $\varphi = 90^\circ$:

$$\varepsilon_{90^\circ\psi}^S = \frac{1}{2} S_2^{hkl} \langle \sigma_{22}^S \rangle \sin^2 \psi + S_1^{hkl} (\langle \sigma_{11}^S \rangle + \langle \sigma_{22}^S \rangle). \quad (50)$$

For $\varphi = 45^\circ$:

$$\begin{aligned} \varepsilon_{45^\circ\psi}^S = & \frac{1}{2} S_2^{hkl} \left(\frac{\langle \sigma_{11}^S \rangle + \langle \sigma_{22}^S \rangle}{2} + \langle \sigma_{12}^S \rangle \right) \sin^2 \psi \\ & + S_1^{hkl} (\langle \sigma_{11}^S \rangle + \langle \sigma_{22}^S \rangle). \end{aligned} \quad (51)$$

The slopes deduced from the straight lines drawn through the data in the three $\sin^2 \psi$ plots [according to equations (49)–(51)] for $\varphi = 0, 45$ and 90° , respectively, present a set of three

equations from which the three stress components $\langle \sigma_{11}^S \rangle$, $\langle \sigma_{22}^S \rangle$ and $\langle \sigma_{12}^S \rangle$ can be calculated in a straightforward manner following equations (46) and (47) (with $\langle \sigma_{33}^S \rangle = 0$).

4.1.4. $\sin^2 \psi$ method: analysis of a biaxial principal stress state. For a biaxial state of stress, *i.e.* non-zero and unequal components $\langle \sigma_{11}^S \rangle$ and $\langle \sigma_{22}^S \rangle$ (stress perpendicular to the surface, $\langle \sigma_{33}^S \rangle$, is zero), the strain–stress relation, equation (16), becomes

$$\begin{aligned} \varepsilon_{\varphi\psi}^{hkl} = & \frac{1}{2} S_2^{hkl} (\cos^2 \varphi \langle \sigma_{11}^S \rangle + \sin^2 \varphi \langle \sigma_{22}^S \rangle) \sin^2 \psi \\ & + S_1^{hkl} (\langle \sigma_{11}^S \rangle + \langle \sigma_{22}^S \rangle). \end{aligned} \quad (52)$$

In this case two series of measurements have to be performed along the principal axes in the sample plane, *i.e.* at $\varphi = 0$ and 90° .

For $\varphi = 0^\circ$, equation (52) reads:

$$\varepsilon_{0^\circ\psi}^{hkl} = \frac{1}{2} S_2^{hkl} \langle \sigma_{11}^S \rangle \sin^2 \psi + S_1^{hkl} (\langle \sigma_{11}^S \rangle + \langle \sigma_{22}^S \rangle). \quad (53)$$

For $\varphi = 90^\circ$:

$$\varepsilon_{90^\circ\psi}^S = \frac{1}{2} S_2^{hkl} \langle \sigma_{22}^S \rangle \sin^2 \psi + S_1^{hkl} (\langle \sigma_{11}^S \rangle + \langle \sigma_{22}^S \rangle). \quad (54)$$

The lattice strain is measured for several angles ψ at $\varphi = 0$ and 90° .

The two plots of $\varepsilon_{0^\circ\psi}^{hkl}$ and $\varepsilon_{90^\circ\psi}^{hkl}$, respectively, *versus* $\sin^2 \psi$ lead to straight lines and the (principal) stresses $\langle \sigma_{11}^S \rangle$ and $\langle \sigma_{22}^S \rangle$ are obtained from the slopes.

4.1.5. $\sin^2 \psi$ method: analysis of a rotationally symmetric biaxial stress state. For a rotationally symmetric biaxial state of stress the non-zero components of the stress tensor are $\langle \sigma_{11}^S \rangle = \langle \sigma_{22}^S \rangle = \langle \sigma_{\parallel}^S \rangle$ (stress perpendicular to the surface, $\langle \sigma_{33}^S \rangle$, is zero) and the general strain–stress relation, equation (16), reduces to (there is no φ dependence):

$$\varepsilon_{\psi}^{hkl} = (2 S_1^{hkl} + \frac{1}{2} S_2^{hkl} \sin^2 \psi) \langle \sigma_{\parallel}^S \rangle. \quad (55)$$

The strain ε_{ψ}^{hkl} is measured at several ψ angles. When ε_{ψ}^{hkl} is plotted *versus* $\sin^2 \psi$, a straight line is obtained and the stress $\langle \sigma_{\parallel}^S \rangle$ can be deduced from the slope.

4.1.6. $\sin^2 \psi$ method: analysis of a uniaxial stress state. For a uniaxial state of stress, the only non-zero component of the stress tensor is $\langle \sigma_{11}^S \rangle$ and the general strain–stress relation, equation (16), reduces to

$$\varepsilon_{\varphi\psi}^{hkl} = S_1^{hkl} \langle \sigma_{11}^S \rangle + \frac{1}{2} S_2^{hkl} \sin^2 \psi (\langle \sigma_{11}^S \rangle \cos^2 \varphi). \quad (56)$$

The strain $\varepsilon_{\varphi\psi}^{hkl}$ is measured at several ψ angles at $\varphi = 0^\circ$. When $\varepsilon_{\varphi\psi}^{hkl}$ is plotted *versus* $\sin^2 \psi$, a straight line is obtained and the stress $\langle \sigma_{11}^S \rangle$ can be deduced from the slope.

The diffraction stress analyses discussed until now for the triaxial case and the different simplifications employ at most three different φ angles; *i.e.* the ψ angle is the predominant angle for the variation of the strain measurement direction. Two methods for stress analysis employing predominantly variation of the measurement direction by φ angle variation are discussed next.

4.1.7. φ integral method: analysis of a triaxial stress state. The strain $\varepsilon_{\varphi\psi}^{hkl}$ in equation (13), being a function of φ with period 2π , can be conceived as a Fourier series in φ up to the second order (Lode & Peiter, 1981; Wagner *et al.*, 1983):

$$\varepsilon_{\varphi\psi}^{hkl} = \sum_{n=0}^2 A_n(\psi) \cos(n\varphi) + B_n(\psi) \sin(n\varphi), \quad (57)$$

with Fourier coefficients²

$$A_0(\psi) = (\varepsilon_{11}^S + \varepsilon_{22}^S) \sin^2 \psi + 2 \varepsilon_{33}^S \cos^2 \psi, \quad (58)$$

$$A_1(\psi) = \varepsilon_{13}^S \sin(2\psi), \quad (59)$$

$$A_2(\psi) = \frac{1}{2} (\varepsilon_{11}^S - \varepsilon_{22}^S) \sin^2 \psi, \quad (60)$$

$$B_1(\psi) = \varepsilon_{23}^S \sin(2\psi) \quad (61)$$

and

$$B_2(\psi) = \varepsilon_{12}^S \sin^2 \psi. \quad (62)$$

Hence, the Fourier coefficients $A_n(\psi)$ and $B_n(\psi)$ can be calculated by Fourier inversion of equation (57) from the strain values $\varepsilon_{\varphi\psi}^{hkl}$ measured at a fixed ψ angle in the interval $\varphi = 0-2\pi$:

$$A_n(\psi) = \frac{1}{\pi} \int_0^{2\pi} \varepsilon_{\varphi\psi}^{hkl} \cos(n\varphi) d\varphi \quad (63)$$

and

$$B_n(\psi) = \frac{1}{\pi} \int_0^{2\pi} \varepsilon_{\varphi\psi}^{hkl} \sin(n\varphi) d\varphi. \quad (64)$$

Employing equations (63) and (64) for at least two ψ angles, all of the six independent components ε_{ij}^S of the strain tensor can be calculated from equations (58) to (62). The entire components $\langle \sigma_{ij}^S \rangle$ of the stress tensor are then obtained from Hooke's law [see also equation (9) with S_1 and $\frac{1}{2}S_2$ substituted by S_1^{hkl} and $\frac{1}{2}S_2^{hkl}$]:

$$\langle \sigma_{ij}^S \rangle = \frac{1}{\frac{1}{2}S_2^{hkl}} \left[\varepsilon_{ij}^S + \frac{-S_1^{hkl}}{\frac{1}{2}S_2^{hkl} + 3S_1^{hkl}} (\varepsilon_{11}^S + \varepsilon_{22}^S + \varepsilon_{33}^S) \delta_{ij} \right]. \quad (65)$$

The reliability of the results can be improved by measuring at more than two values of ψ . Then [instead of solving directly equations (58) to (62)] a least-squares optimization procedure has to be adopted for the determination of the components of the strain tensor ε_{ij}^S .

4.1.8. $\cos^2\varphi$ method: analysis of a biaxial stress state. Substituting $\sin^2\varphi$ by $1 - \cos^2\varphi$ in equation (48), the simplification of equation (16) for the stress state considered becomes

$$\varepsilon_{\varphi\psi}^{hkl} = \frac{1}{2} S_2^{hkl} \left[\cos^2 \varphi (\langle \sigma_{11}^S \rangle - \langle \sigma_{22}^S \rangle) + \sin(2\varphi) \langle \sigma_{12}^S \rangle + \langle \sigma_{22}^S \rangle \right] \sin^2 \psi + S_1^{hkl} (\langle \sigma_{11}^S \rangle + \langle \sigma_{22}^S \rangle). \quad (66)$$

For a fixed value of ψ , values for the parameters c_{ψ}^+ and c_{ψ}^- , as determined by the strains $\varepsilon_{\varphi>0\psi}^{hkl}$ and $\varepsilon_{\varphi<0\psi}^{hkl}$, with $|\varphi|$ constant, *i.e.* measured at positive and negative values of the angle φ , respectively, are obtained from (see Ballard *et al.*, 1997)

$$\begin{aligned} c_{\psi}^+ &= \frac{1}{2} (\varepsilon_{\varphi>0\psi}^{hkl} + \varepsilon_{\varphi<0\psi}^{hkl}) \\ &= \frac{1}{2} S_2^{hkl} (\langle \sigma_{11}^S \rangle - \langle \sigma_{22}^S \rangle) \sin^2 \psi \cos^2 \varphi + \frac{1}{2} S_2^{hkl} \langle \sigma_{22}^S \rangle \sin^2 \psi \\ &\quad + S_1^{hkl} (\langle \sigma_{11}^S \rangle + \langle \sigma_{22}^S \rangle) \end{aligned} \quad (67)$$

and

$$c_{\psi}^- = \frac{1}{2} (\varepsilon_{\varphi>0\psi}^{hkl} - \varepsilon_{\varphi<0\psi}^{hkl}) = \frac{1}{2} S_2^{hkl} \langle \sigma_{12}^S \rangle \sin^2 \psi \sin(2\varphi). \quad (68)$$

Note that with this representation, *i.e.* by c_{ψ}^+ and c_{ψ}^- , the shear component $\langle \sigma_{12}^S \rangle$ is treated independently of the other stress tensor components.

For a fixed value of ψ and for a given reflection hkl , lattice strains are measured for several pairs of positive and negative values of the angle φ (*i.e.* with $|\varphi|$ constant). Then a plot of c_{ψ}^+ versus $\cos^2\varphi$ leads to a straight line (Fig. 8). The slope, C_{ψ}^+ , and the intercept with the c_{ψ}^+ axis, I_{ψ}^+ , provide two equations for the stress components $\langle \sigma_{11}^S \rangle$ and $\langle \sigma_{22}^S \rangle$, which can be solved as

$$\langle \sigma_{22}^S \rangle = \frac{1}{2 S_1^{hkl} + \frac{1}{2} S_2^{hkl} \sin^2 \psi} \left(I_{\psi}^+ - \frac{C_{\psi}^+ S_1^{hkl}}{\frac{1}{2} S_2^{hkl} \sin^2 \psi} \right) \quad (69)$$

and

$$\langle \sigma_{11}^S \rangle = \frac{C_{\psi}^+}{\frac{1}{2} S_2^{hkl} \sin^2 \psi} + \langle \sigma_{22}^S \rangle. \quad (70)$$

The plot of c_{ψ}^- versus $\sin(2\varphi)$ leads to a straight line (with zero offset). The stress $\langle \sigma_{12}^S \rangle$ is deduced from the slope (Fig. 8).

In the case that the stress state is a principal biaxial stress state, the plot of c_{ψ}^- versus $\sin(2\varphi)$ is superfluous as $\langle \sigma_{12}^S \rangle$ is equal to zero.

4.2. Multiple hkl reflections

By measuring lattice strain using different reflections hkl , *i.e.* by measuring at different Bragg angles θ^{hkl} , the direction of the lattice strain measurement can be varied without tilting the specimen physically in the diffractometer [cf. §3, equation (25)]. This is important (i) for the application of grazing-incidence diffraction where the fixed (and small) angle of incidence of the X-ray beam poses restrictions for the angle ψ , and (ii) for large samples that can be mounted, but not tilted in the diffractometer.

However, the following methods can also be used in cases where specimen tilt is possible.

4.2.1. $g(\psi, hkl)$ method: analysis of a biaxial stress state. In an evaluation of the stress from lattice strain measurements for different reflections hkl , the dependence of the strain ε_{ψ}^{hkl} on hkl has to be dealt with, which requires a modification of the $\sin^2\psi$ plot. Equation (48) [*i.e.* the simplification of equation (16) for a biaxial stress state] can be reformulated by introducing

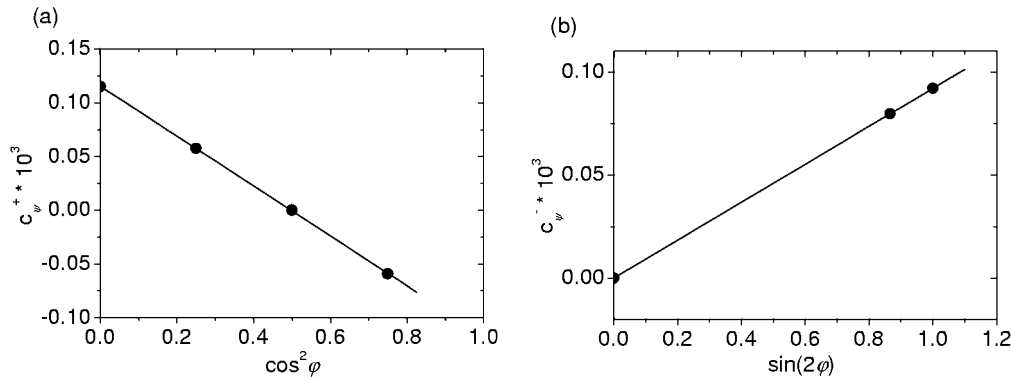
$$g(\psi, hkl) = \frac{1}{2} \frac{S_2^{hkl}}{S_1^{hkl}} \sin^2 \psi. \quad (71)$$

Thus, for $\varphi = 0^\circ$:

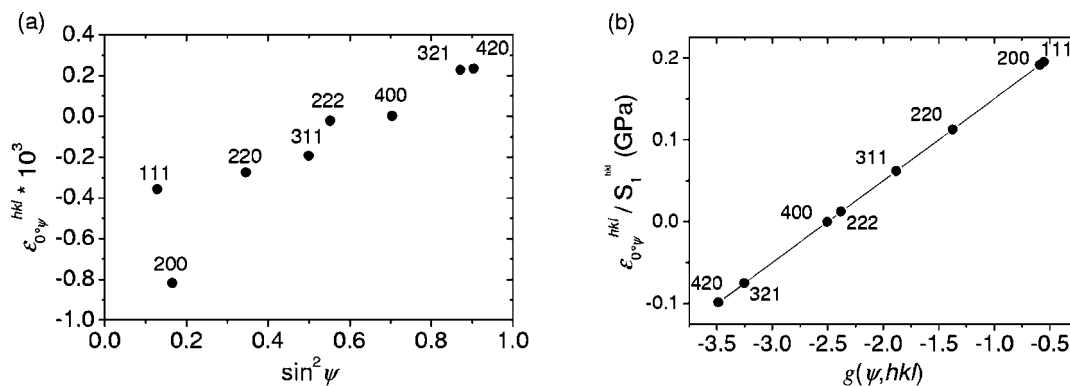
$$\varepsilon_{0-\psi}^{hkl} = g(\psi, hkl) \langle \sigma_{11}^S \rangle + (\langle \sigma_{11}^S \rangle + \langle \sigma_{22}^S \rangle). \quad (72)$$

For $\varphi = 90^\circ$:

² Note that the components of the strain tensor ε_{ij}^S should be written as $\{\varepsilon_{ij}^S\}^{hkl}$. For the sake of simplicity, the curly brackets and the indication of the reflection are omitted.


Figure 8

Stress analysis employing the $\cos^2\varphi$ method: calculated example. (a) Plot of c_{45}^+ versus $\cos^2\varphi$ and (b) plot of c_{45}^- versus $\sin(2\varphi)$ for the 331 reflection of a macroscopically elastically isotropic copper specimen subjected to the mechanical stress state with $\langle\sigma_{11}^S\rangle = 100$ MPa, $\langle\sigma_{22}^S\rangle = 150$ MPa and $\langle\sigma_{12}^S\rangle = \langle\sigma_{21}^S\rangle = 20$ MPa (all other components are zero). For details, see text.


Figure 9

Stress analysis employing the $g(\psi, hkl)$ method: calculated example. Lattice strain for the 111, 200, 220, 311, 222, 400, 321 and 420 reflections of a macroscopically elastically isotropic copper specimen subjected to the mechanical stress state with $\langle\sigma_{11}^S\rangle = 100$ MPa, $\langle\sigma_{22}^S\rangle = 150$ MPa and $\langle\sigma_{12}^S\rangle = \langle\sigma_{21}^S\rangle = 20$ MPa (all other components equal to zero): (a) 'classical' plot of $\varepsilon_{0^\psi}^{hkl}$ versus $\sin^2\psi$ and (b) plot of $\varepsilon_{0^\psi}^{hkl}/S_1^{hkl}$ versus $g(\psi, hkl)$. Tilt angles for the individual reflections as shown in (a) would be obtained if a measurement is conducted as a 2θ scan at a fixed small incidence angle (*cf.* §3). For details, see text.

$$\frac{\varepsilon_{90^\psi}^{hkl}}{S_1^{hkl}} = g(\psi, hkl)\langle\sigma_{22}^S\rangle + (\langle\sigma_{11}^S\rangle + \langle\sigma_{22}^S\rangle). \quad (73)$$

For $\varphi = 45^\circ$:

$$\frac{\varepsilon_{45^\psi}^{hkl}}{S_1^{hkl}} = g(\psi, hkl)\left(\frac{\langle\sigma_{11}^S\rangle + \langle\sigma_{22}^S\rangle}{2} + \langle\sigma_{12}^S\rangle\right) + \langle\sigma_{11}^S\rangle + \langle\sigma_{22}^S\rangle. \quad (74)$$

The strain is measured at three angles $\varphi = 0, 90$ and 45° for (one or) several reflections hkl and (hypothetically one or) several angles ψ . The stresses $\langle\sigma_{11}^S\rangle$ and $\langle\sigma_{22}^S\rangle$ are obtained directly from the slopes of straight lines obtained by plotting $\varepsilon_{0^\psi}^{hkl}/S_1^{hkl}$ and $\varepsilon_{90^\psi}^{hkl}/S_1^{hkl}$, respectively, versus $g(\psi, hkl)$ (see Fig. 9 for an example), and the shear component $\langle\sigma_{12}^S\rangle$ is calculated from the slope of the straight line obtained by plotting $\varepsilon_{45^\psi}^{hkl}/S_1^{hkl}$ versus $g(\psi, hkl)$. This method of diffraction stress analysis has been proposed recently by Vermeulen (2002).

A straightforward simplification of the above-described method is possible for the case of a biaxial principal state of stress ($\langle\sigma_{12}^S\rangle = 0$). In this case, measurements at $\varphi = 0$ and 90° for one or several reflections hkl and for several angles ψ suffice for the determination of the stresses $\langle\sigma_{11}^S\rangle$ and $\langle\sigma_{22}^S\rangle$.

A simplification of this method is possible for a rotationally symmetric biaxial state of stress, which will be discussed next.

4.2.2. $f(\psi, hkl)$ method: analysis of a rotationally symmetric biaxial state of stress. Equation (55) [*i.e.* the simplification of equation (16) for a rotationally symmetric biaxial stress state] can be written as (Quaeyhaegens *et al.*, 1995; Kamminga, de Keijser *et al.*, 2000)

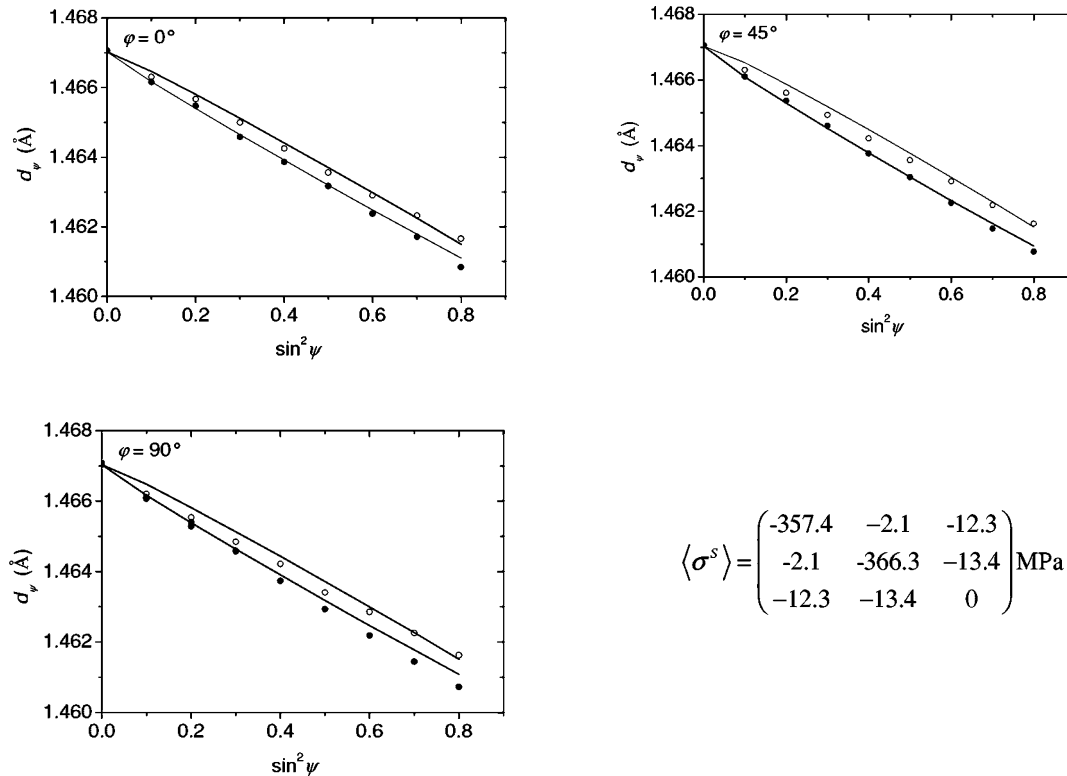
$$\varepsilon_{\psi}^{hkl} = f(\psi, hkl)\langle\sigma_{\parallel}^S\rangle \quad (75)$$

with

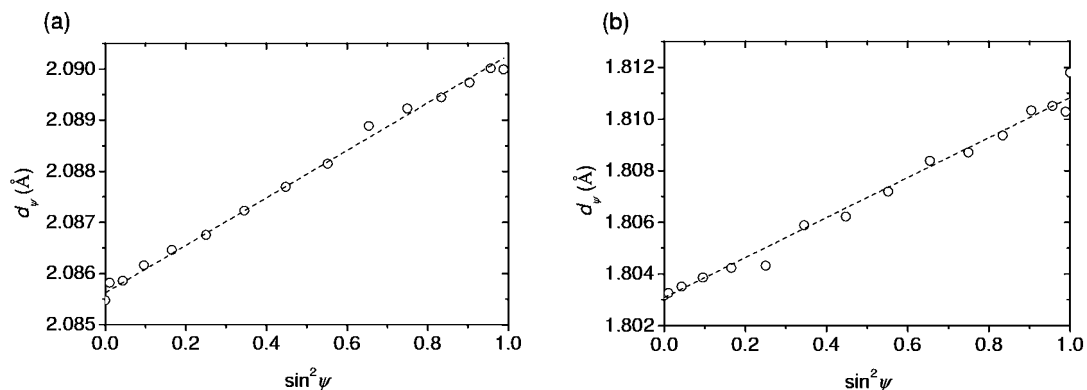
$$f(\psi, hkl) = 2S_1^{hkl} + \frac{1}{2}S_2^{hkl}\sin^2\psi. \quad (76)$$

In the references mentioned, only cubic materials were considered. In this case, equation (75) expressed in terms of the lattice constant a can be applied (*cf.* Vermeulen, 2002).

The strain ε_{ψ}^{hkl} can be measured for (one or) several reflections hkl at (hypothetically one or) several ψ angles. Then a plot of ε_{ψ}^{hkl} versus $f(\psi, hkl)$ leads to a straight line (offset = 0) and the stress $\langle\sigma_{\parallel}^S\rangle$ is given by the slope (Fig. 10).


Figure 11

Stress analysis employing a general least-squares analysis: practical example. Lattice spacing for the 013 reflection of a macroscopically elastically isotropic Zircaloy specimen at three different rotation angles φ (0, 45 and 90°) measured at positive (open circles) and negative (full circles) specimen tilt. Fitting was performed using five independent stress tensor components: $\langle \sigma_{11}^S \rangle$, $\langle \sigma_{22}^S \rangle$, $\langle \sigma_{23}^S \rangle$, $\langle \sigma_{13}^S \rangle$, $\langle \sigma_{33}^S \rangle$ ($\langle \sigma_{33}^S \rangle$ was set to zero); the calculated lattice strains are indicated by the lines in the figure. In addition, the strain-free lattice spacing for the {013} planes was used as a fit parameter in order to fit data on the basis of lattice spacing instead of lattice strains. The results are indicated by the stress tensor in the figure. The error for the diagonal components is 10 MPa; the error for the off-diagonal components is 2 MPa. The strain-free lattice spacing is used only as a dummy parameter. It could be used for the determination of the strain-free lattice constants only after correction for instrumental aberrations (*cf.* §4.4.1).


Figure 12

Stress analysis employing a general least-squares analysis: practical example. Lattice spacing for the 111 (a) and 200 (b) reflections of a macroscopically elastically isotropic copper specimen (practically untextured thin film of thickness of about 0.5 μm , produced by physical vapour deposition). Fitting was performed using one independent stress tensor component: $\langle \sigma_{11}^S \rangle = \langle \sigma_{22}^S \rangle$ (all other components are zero). In addition, the strain-free lattice spacings for the {111} and {200} planes were used as fit parameters in order to fit data on the basis of lattice spacing instead of lattice strains. The result is: $\langle \sigma_{11}^S \rangle = \langle \sigma_{22}^S \rangle = 282 \pm 7$ MPa. The strain-free lattice spacings are used only as dummy parameters. They could be used for the determination of the strain-free lattice constants only after correction for instrumental aberrations (*cf.* §4.4.1).

of the $\{hkl\}$ lattice planes can be directly obtained [equation (2)], whereas the lattice strain has to be calculated from [*cf.* equation (3)]

$$\varepsilon_{\varphi\psi}^{hkl} = \frac{d_{\varphi\psi}^{hkl} - d_0^{hkl}}{d_0^{hkl}} \quad (78)$$

with d_0^{hkl} as the strain-free lattice spacing of the $\{hkl\}$ planes. Equation (78) deserves some discussion with respect to possible errors. From equation (78), it follows that

$$\Delta(\varepsilon_{\varphi\psi}^{hkl}) = -\cot(\theta_{\varphi\psi}^{hkl})\Delta(\theta_{\varphi\psi}^{hkl}) - \Delta(d_0^{hkl})/d_0^{hkl}, \quad (79)$$

i.e. errors (deviations) $\Delta(\varepsilon_{\varphi\psi}^{hkl})$ can be due to errors in the measured peak positions or in the values used for the strain-free lattice spacings.

A small error in the strain-free lattice spacing can cause a relatively large error in the strain. As the strains in the elastic regime are usually very small (<0.1%), the lattice spacings have to be known with an accuracy better than of the order of 0.01%. In principle, strain-free lattice spacings can be determined by measuring a strain-free reference sample of the same material as the sample under investigation. However, this can be problematic in practice; for example, strain-free powders of f.c.c. metals, prepared by filing and subsequent annealing, usually contain stacking faults which give rise to shifts of the measured Bragg angles. It is even impossible for materials where the chemical composition or the amount of impurities is not exactly known or for thin films consisting of a metastable phase which cannot be produced as a strain-free bulk (or powder) reference sample. In particular, the exploration of stress gradients can be complicated in the presence of a gradient of the strain-free lattice spacing, *e.g.* due to a non-uniform chemical composition (see, for example, Somers & Mittemeijer, 1990).

An apparent strain-free lattice spacing d_0^{hkl} can be determined directly from the measurement of the strained sample. It is given by the measured lattice spacing at those angles φ and ψ for which, according to the theory, the strain is expected to be zero. In the case of a rotationally symmetric biaxial state of stress, for example, the direction, ψ^* , of zero strain is given by $\sin^2 \psi^* = -2S_1^{hkl} / (\frac{1}{2} S_1^{hkl})$ [*cf.* equation (55)]. A detailed discussion of the stress-free direction for more complicated stress states and the relation with the stress component $\langle \sigma_{33}^S \rangle$ can be found in the textbook by Hauk (1997, §2.11 therein). In the case of the presence of instrumental errors or imprecisely known elastic constants, the thus determined apparent strain-free lattice constant deviates from the true value. The elastic constants are not required if lattice spacings are measured under different load stresses. The strain-free direction, ψ^* , and the strain-free lattice spacing, d_0^{hkl} , are given by the intersection point of the $d_{\varphi\psi}^{hkl}$ versus $\sin^2 \psi$ plots for different load stresses. For an investigation of invariant intersections in diffraction stress analysis, see Hauk & Krüger (2000).

The error in the angular position, $\theta_{\varphi\psi}^{hkl}$, of a diffraction line is caused by instrumental aberrations. Peak shifts due to instrumental aberrations can be, even for a well maintained diffractometer, of the order of the peak shifts arising due to the presence of stresses [for a detailed discussion on the effect of instrumental errors in diffraction stress analysis, see, for example, Noyan & Cohen (1987), Vermeulen (2000), Vermeulen & Houtman (2000), and Leoni *et al.* (2004)]. Some instrumental effects cause ψ -independent errors of the peak position (*e.g.* zero-offset of the 2θ scale, cradle-axis misalignment); *i.e.* peak shifts, but no absolute peak positions can be reliably measured. Other instrumental effects cause ψ -dependent errors of the peak position (*e.g.* incident-beam misalignment and specimen height displacement); *i.e.* neither peak shifts nor absolute peak positions can be reliably measured. It is useful to distinguish between errors leading to

$\Delta(\varepsilon_{\varphi\psi}^{hkl})$ independent of ψ , in the following referred to as errors of the first kind, and those leading to a $\Delta(\varepsilon_{\varphi\psi}^{hkl})$ depending on ψ , in the following referred to as errors of the second kind: the different analysis methods, as discussed in this review, have different susceptibilities to the two kinds of errors (see what follows).

A constant error $\Delta(\varepsilon_{\varphi\psi}^{hkl})$ is only possible if the instrumental error $\Delta(\theta_{\varphi\psi}^{hkl})$ is constant (*e.g.* zero-offset of the 2θ scale, cradle-axis misalignment) and only one reflection [only one $\cot(\theta_{\varphi\psi}^{hkl})$ in equation (79)] is used, or, in case of multiple hkl , if $\Delta(\theta_{\varphi\psi}^{hkl}) = 0$ and $\Delta(d_0^{hkl})/d_0^{hkl} = \text{constant}$ (independent of hkl). The error in the strain-free lattice spacing, $\Delta(d_0^{hkl})/d_0^{hkl}$, is constant for cubic systems (given by the error of the cell parameter), whereas for all other crystal systems (involving several cell parameters) it can depend on the reflection hkl .

Methods for the determination of the complete stress tensor; methods involving more than one hkl reflection; $\cos^2 \varphi$ method. These methods require the knowledge of absolute strains $\varepsilon_{\varphi\psi}^{hkl}$ and the result of such an evaluation is susceptible to both kinds of instrumental errors. As an example, it can be deduced from equations (35)–(40) for the method of analysis described in §4.1.1 (triaxial stress state), that only the determination of the hydrostatic component $\sigma_h = \frac{1}{3}(\langle \sigma_{11}^S \rangle + \langle \sigma_{22}^S \rangle + \langle \sigma_{33}^S \rangle)$ of the stress tensor requires the knowledge of absolute strains (and thus of absolute peak positions), whereas the deviatoric components are calculated employing only changes in strain (and thus shifts of peaks).

If the presence of instrumental errors leading to an error of the second kind $\Delta(\varepsilon_{\varphi\psi}^{hkl})$ cannot be excluded, it is generally recommended to determine separately an (apparent) strain-free lattice spacing, $d_{0,\varphi\psi}^{hkl}$, for all φ , ψ angles (and hkl reflections) involved in the analysis. This can be accomplished by using a strain-free reference sample composed of the same material as the sample under investigation (see, for example, van Leeuwen *et al.*, 1999). In this case, the lattice strain has to be calculated from

$$\varepsilon_{\varphi\psi}^{hkl} = \frac{d_{\varphi\psi}^{hkl} - d_{0,\varphi\psi}^{hkl}}{d_{0,\varphi\psi}^{hkl}}, \quad (80)$$

where the errors due to instrumental effects cancel out.

Alternative correction procedures involve analytical expressions for the instrumental errors; see, for example, Vermeulen & Houtman (2000) and Vermeulen (2000).

Methods for the determination of the stress tensor with $\langle \sigma_{33}^S \rangle = 0$, involving only one hkl reflection. For the case that $\langle \sigma_{33}^S \rangle$ can be assumed to be zero, the methods employing only one particular hkl reflection are susceptible to errors of the second kind only (except the $\cos^2 \varphi$ method; see above). These methods do not require the knowledge of absolute strains: relative strains suffice. The stress tensor components are not influenced by an error of the first kind, because they are determined from the slopes of plots of the strain versus ψ (or functions of ψ), such slopes not being affected by this kind of error.

It should be noted that also in the general least-squares fitting (§4.3), errors of the first kind $\Delta(\varepsilon_{\varphi\psi}^{hkl})$ play no role if

appropriate parameters, such as an apparent strain-free lattice spacing, are included in the fit.

As a concluding remark, it is noted that an appropriate choice of the diffractometer optics can substantially reduce the significance of tilting-related instrumental errors. For example, the use of parallel-beam optics may be preferred over the use of focusing optics for precise stress measurements (Leoni *et al.*, 2004).

4.4.2. Miscellaneous. It is worth noting that the $\cos^2\varphi$ method (§4.1.8) is performed at a single angle ψ . So absolute values of the strains are needed for the determination of the stresses (in contrast to the $\sin^2\psi$ method, for example, where the stress is determined from the slope of a plot of $\varepsilon_{\varphi\psi}^{hkl}$ versus $\sin^2\psi$). If the actual stress-free lattice spacing of the sample is different from the theoretical value, *e.g.* due to impurities, errors in the stress values occur. For this reason, it is recommended to determine experimentally the stress-free value $d_{0,\varphi\psi}^{hkl}$ (see above).

With methods where X-ray elastic constants for at least two reflections are involved in the calculation of a stress component from a slope in a specific plot [$f(\psi, hkl)$ and $g(\psi, hkl)$ methods], the criterion of linear behaviour of the considered plot allows one to check if these XECs are consistent with the investigated sample (see *e.g.* Vermeulen, 2002).

For cases where the principal axes of the state of stress are unknown, an elliptical regression using various $\varepsilon_{\varphi\psi}^{hkl}$ measurements should be preferred rather than a linear regression in order to determine shear stress components, as this method handles the data more appropriately with respect to counting statistics (*cf.* Fig. 11 for an experimental example).

4.4.3. Available methods for grazing-incidence diffraction.

For the case of grazing-incidence diffraction, the constraint of a small and fixed incidence angle restricts the number of applicable stress analysis methods (as described in §4 for macroscopically isotropic materials) to the following cases.

(i) Wavelength fixed, variation of ψ by use of multiple hkl : $f(\psi, hkl)$ method (see §4.2.2) for a rotationally symmetric biaxial state of stress, or $g(\psi, hkl)$ method (see §4.2.1) for a biaxial state of stress.

(ii) hkl fixed, variation of ψ by use of different wavelengths: $\cos^2\varphi$ method (§4.1.8) for a plane state of stress, or φ integral method (§4.1.7) for a triaxial state of stress.

5. Macroscopically elastically anisotropic specimens

5.1. Basis

Many specimens investigated by diffraction stress analysis are not macroscopically elastically isotropic and, thus, the methods of analysis described in §4 cannot, in principle, be employed. Two sources of macroscopic elastic anisotropy can be conceived: the occurrence of crystallographic texture (for an overview, see, for example, Hauk, 1997) and the occurrence of direction-dependent elastic grain interaction (van Leeuwen *et al.*, 1999; Welzel & Mittemeijer, 2003; Welzel *et al.*, 2003; Koch *et al.*, 2004; Welzel, Leoni & Mittemeijer, 2004; for an

overview of various grain-interaction models, see Appendix A).

For decades, only texture³ was considered as a possible source of macroscopic elastic anisotropy, although the impact of direction-dependent grain interaction on diffraction stress analysis was discussed by Stickforth as long ago as 1966 (Stickforth, 1966), in particular in view of the occurrence of a free surface for crystallites located within the surface region of a polycrystalline aggregate. Direction-dependent grain interaction due to the occurrence of a free surface is called ‘surface anisotropy’. Until recently, experimental investigations yielded no evidence for the occurrence of ‘surface anisotropy’ in the stress analysis of surface regions of bulk materials by X-ray diffraction (for an overview, see Hauk, 1997). Only recently (van Leeuwen *et al.*, 1999; Welzel *et al.*, 2003), it was demonstrated for the first time experimentally that, at least in thin films, direction-dependent grain interaction can significantly influence the dependence of lattice strain on the direction of observation (see §5.2.2 and §A5.2; see, in particular, Welzel, Leoni & Mittemeijer, 2004). It was also shown very recently that the occurrence of a grain-shape (morphological) texture results in direction-dependent grain interaction and thus in macroscopic elastic anisotropy (Koch *et al.*, 2004).

In the case of a macroscopically elastically anisotropic specimen, the so-called diffraction (X-ray) stress factors have to be used for diffraction stress analysis [*cf.* equation (17) and its discussion in §2; see also Welzel & Mittemeijer, 2003]:

$$\{\varepsilon_{33}^L\}_{\varphi\psi}^{hkl} = F_{ij}(\varphi, \psi, hkl)\langle\sigma_{ij}^S\rangle. \quad (81)$$

Whereas diffraction stress analysis for macroscopically elastically isotropic (quasi-isotropic) specimens on the basis of equation (16) has been extensively performed in the past, only a very limited number of investigations have been dedicated to macroscopically elastically anisotropic specimens. The consequence of texture on diffraction stress analysis has not generally been treated in review papers (*cf.* Table 1). This may be owing to the complications caused by the occurrence of macroscopic elastic anisotropy: the texture has to be described quantitatively, *i.e.* either in terms of ideal orientations or in terms of the orientation distribution function, and/or an appropriate direction-dependent grain-interaction model is required.

When the texture is very sharp and strong, it may be described by single-crystal-like ideal orientations. The corresponding diffraction stress analysis method is called the crystallite group method (Willemsse & Naughton, 1985; Willemsse *et al.*, 1982; Hauk & Vaessen, 1985; Hauk, 1986; Hauk & Oudelhoven, 1988; Baron & Hauk, 1988). In this limit, single-crystal elastic compliances can be used and grain interaction can be ignored, *i.e.* adoption of a grain-interaction model is not necessary.

³ The notion texture without further specification refers to the occurrence of crystallographic, not morphological, texture in the following.

The general case of diffraction stress analysis for macroscopically elastically anisotropic samples is dealt with in §5.2. The crystallite group method is discussed in §5.3.

5.2. General least-squares analysis of any stress state for macroscopically elastically anisotropic specimens

Results of strain measurements for macroscopically elastically anisotropic specimens are usually presented, in analogy to the quasi-isotropic case, as plots of lattice strain *versus* $\sin^2 \psi$. Generally, non-linear $\sin^2 \psi$ plots are obtained for macroscopically elastically anisotropic specimens due to the presence of crystallographic texture and/or direction-dependent grain interaction.

In the case of texture and in the absence of direction-dependent grain interaction, with respect to the appearance of curvature in the $\sin^2 \psi$ plots, the only exceptions are the $\sin^2 \psi$ plots for the *hhh* and *h00* reflections of cubic materials where linear $\sin^2 \psi$ plots occur (Dölle & Hauk, 1979; Brakman, 1983). Although for these exceptions, formally, φ, ψ -independent diffraction elastic constants S_1^{hkl} and $\frac{1}{2}S_2^{hkl}$ can be defined, their values are generally texture dependent, and thus texture also has to be considered. Hence an analysis performed by employing the corresponding diffraction (X-ray) elastic constants S_1^{hkl} and $\frac{1}{2}S_2^{hkl}$, which are only valid for the untextured case, is not recommended.

In the case of *direction-dependent grain interaction*, non-linear $\sin^2 \psi$ plots are always obtained (provided that single-crystal elastic anisotropy occurs). Whereas most of the methods for stress analysis of quasi-isotropic specimens rely on a few measured lattice strains (for a few ψ angles) for each φ angle for a given *hkl* reflection (typically five to ten lattice-strain measurements for a fixed φ and a particular *hkl* reflection), for macroscopically elastically anisotropic specimens, the data sampled as a function of ψ (or $\sin^2 \psi$) should be much more dense in order to resolve the non-linearities in the $\sin^2 \psi$ behaviour reliably.

When the diffraction (X-ray) stress factors are known, either by measurement or by calculation from single-crystal elastic compliances by adopting a grain-interaction model (*cf.* Appendix A), the unknown stress tensor components can be determined as fit parameters by least-squares minimization of the difference χ^2 of the strains calculated from equation (81), $\varepsilon_i^{calc}(\sigma, hkl, \varphi, \psi)$ and the measured strain, $\varepsilon_i^{meas}(hkl, \varphi, \psi)$, *cf.* equation (77).

In fact, this is the most general solution method which could also be applied in the case of macroscopically elastically isotropic specimens (but in this case the special methods discussed in §4 should be preferred). The relation between the diffraction (X-ray) stress factors and the diffraction (X-ray) elastic constants for *macroscopically elastically isotropic* specimens reads [Hauk, 1997; for the definition of **m**, see equation (14)]:

$$F_{ij}(\psi, \varphi, hkl) = \frac{1}{2}S_2^{hkl} m_i^S m_j^S + S_1^{hkl} \delta_{ij}. \tag{82}$$

The following practical examples illustrate the application of the above-described method for diffraction stress analysis to macroscopically elastically anisotropic specimens.

5.2.1. Example 1: uniaxially loaded cold-rolled deep-drawing ferritic steel sheet. Experimental and calculated diffraction (X-ray) stress factors for a ferritic steel sheet are presented in Fig. 13. The experimental stress factors were obtained by loading the specimen in a tensile testing device mounted on the diffractometer. Experimental details can be found in work by Brakman *et al.* (1988). Theoretical values for

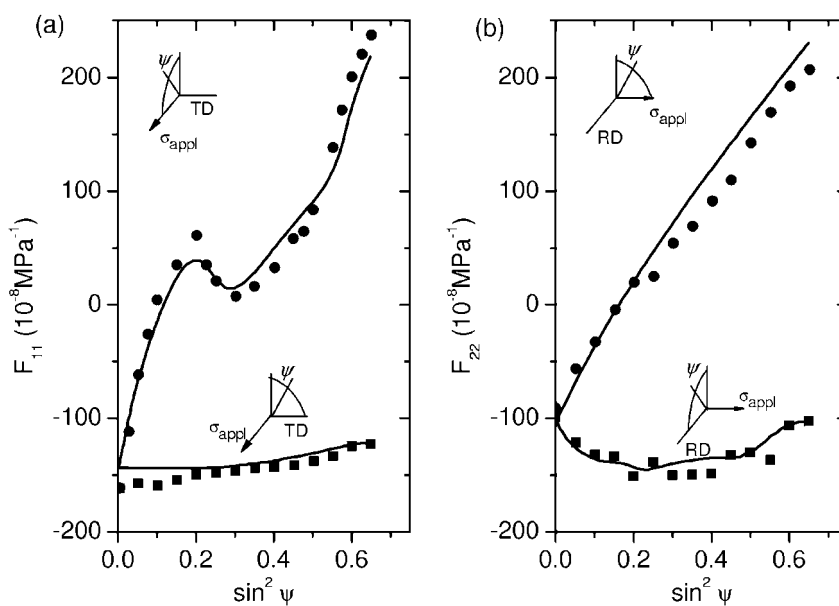


Figure 13 Experimentally determined (symbols) and calculated (lines) X-ray stress factors F_{11} (a) and F_{22} (b) for the 211 reflection of a cold-rolled ferritic steel sheet. The rolling direction (RD), the transverse direction (TD), the loading direction and the direction of strain measurement are indicated in the figure (taken from Brakman *et al.*, 1988).

the stress factors were calculated according to the Neerfeld–Hill model, taking into account the texture information (a rolling texture, in this case) in terms of the orientation distribution function. From Fig. 13 it is evident that both the experimentally determined and the calculated diffraction (X-ray) stress factors exhibit distinct curvature; thus the experimental $\sin^2\psi$ dependence of the stress factors (*i.e.* of the lattice strain) cannot be analysed at all on the basis of a straight-line fit employing the $\sin^2\psi$ formulation as for macroscopically isotropic specimens [equation (16)].

By fitting the lattice strain calculated according to equation (81) to the measured lattice strain as a function of $\sin^2\psi$ by minimizing χ^2 according to equation (77) using the stress tensor components $\langle\sigma_{11}^S\rangle$ and $\langle\sigma_{22}^S\rangle$ as fit parameters, the value of the experimentally applied uniaxial load stress was obtained from the diffraction stress measurement with very good accuracy.

5.2.2. Example 2: textured thin copper layer exhibiting anisotropic elastic grain interaction. Two out of six ε_ψ – $\sin^2\psi$ diagrams as measured by X-ray diffraction are shown in Fig. 14 for a {111} fibre-textured copper film; the corresponding calculated diagrams are also shown (200, 420 shown, 111, 220, 311, 331 not shown). For details of the deposition of the copper layer and the diffraction measurement, together with a detailed treatment of the diffraction stress analysis, see Welzel *et al.* (2003). It was found experimentally that the measured diffraction strain is independent of the sample rotation angle φ , and hence the stress state is rotationally symmetric ($\langle\sigma_{11}^S\rangle = \langle\sigma_{22}^S\rangle$, $\langle\sigma_{12}^S\rangle = 0$). Because the sample surface is unloaded, $\langle\sigma_{33}^S\rangle = 0$. Hence, only $\langle\sigma_{11}^S\rangle = \langle\sigma_{22}^S\rangle$ has to be determined by fitting the lattice strain calculated according to equation (81) to the measured lattice strain as a function of $\sin^2\psi$ by minimizing χ^2 according to equation (77).

From Fig. 14 it is evident that the experimental $\sin^2\psi$ dependence of the lattice strain cannot be analysed on the

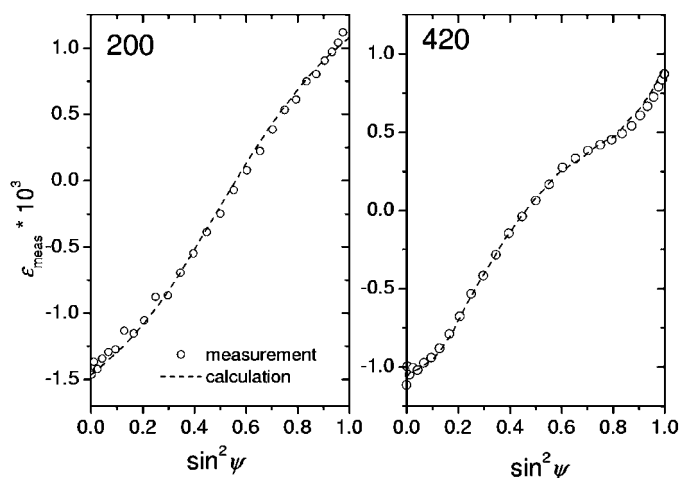


Figure 14 Textured copper film. Measured (open circles) and simulated (dashed line) diffraction strain data for two reflections as function of $\sin^2\psi$ ($\sin^2\psi$ plots). For details of the simulation, see text. The error bars indicating statistical errors on the lattice strains are about twice the size of the circles for the 200 reflection and less than the size of the circles for the 420 reflection.

basis of a straight-line fit employing the $\sin^2\psi$ formulation as for macroscopically isotropic specimens [equation (16)]. It should be noted that all traditional grain-interaction models (*i.e.* the Eshelby–Kröner model and any combination of the Reuss grain-interaction model with the Voigt grain-interaction model, *e.g.* the traditional Neerfeld–Hill model) predict linear $\sin^2\psi$ plots for the $h00$ (and hhh) reflection for textured specimens composed of cubic crystallites; however, the measured $\sin^2\psi$ plot for the 200 reflection in Fig. 14 [and the 111 reflection, not shown in Fig. 14; see Welzel *et al.* (2003)] cannot be described by a straight line. A so-called effective direction-dependent grain-interaction model was developed recently by Welzel *et al.* (2003). Only this direction-dependent grain-interaction model, taking into account the effect of elastic (surface) macroscopic anisotropy of the thin film, is compatible with the curved behaviour in the $\sin^2\psi$ plots observed for the $h00$ (and the hhh , not shown) reflection. By simultaneous fitting of the six measured $\sin^2\psi$ plots, a very satisfactory fit was achieved and a tensile in-plane stress of 165 MPa was determined (for details, see Welzel *et al.*, 2003). Note that for the calculation of the diffraction (X-ray) stress factors, the (fibre-) texture of the specimen was fully taken into account by using the experimentally determined (*i.e.* calculated from measured pole figures) orientation distribution function.

5.3. Special method for textured macroscopically elastically anisotropic specimens: crystallite group method

A method for diffraction stress analysis of macroscopically elastically anisotropic materials with strong and sharp texture components (*i.e.* the orientation distribution function is restricted to a number of localized maxima in Euler space) was proposed by Willems *et al.* (1982) and Willems & Naughton (1985). The method was adapted to rolled specimens by Hauk & Vaessen (1985) (see also Hauk, 1986; Hauk & Oudelhoven, 1988; Welzel & Mittemeijer, 2004) and to fibre-textured specimens by Baron & Hauk (1988). The concept of this method will be revisited next.

In many practical cases, *e.g.* for cold-rolled materials, the texture of a specimen may be described in terms of one or a few so-called ideal orientations (crystallite groups), each consisting of crystallites all with the same crystallographic orientation (*i.e.* an ideal orientation is represented by a set of crystallographically equivalent points in Euler space). Usually, the Miller indices of the crystallographic planes oriented parallel to the sample surface, $\{mnr\}$, and the indices of the S_1 axis of the specimen frame of reference in the crystal frame of reference, (uvw) , are used for defining the orientation of a particular crystallite group.

The strain tensor of a crystallite group in the specimen frame of reference ε^S is related to the stress tensor σ^S by Hooke's law employing single-crystal elastic compliances transformed to the specimen reference frame s_{ijkl}^S :

$$\varepsilon_{ij}^S = s_{ijkl}^S \sigma_{kl}^S. \quad (83)$$

In equation (83), ε_{ij}^S and σ_{kl}^S have to be considered as averages over all (spatially distributed) crystallites in the specimen belonging to the crystallite group under consideration. Equation (83) holds also for the lattice strain measured by diffraction, provided that for the strain measurement, only crystallites of the crystallite group under consideration contribute to a diffraction line.

The measured lattice strain $\varepsilon_{\varphi\psi}$ can be calculated from the strain tensor in the specimen frame of reference, ε^S , and the unit vector, \mathbf{m}^S , in the direction of the diffraction vector as expressed in the specimen frame of reference as follows:

$$\varepsilon_{\varphi\psi} = m_i^S m_j^S \varepsilon_{ij}^S = m_i^S m_j^S s_{ijkl}^S \sigma_{kl}^S. \quad (84)$$

As no distinction of diffraction strain and mechanical strain has to be made for a crystallite group, the symbol $\varepsilon_{\varphi\psi}$, *i.e.* the strain in the direction of the (normalized) diffraction vector in the specimen reference frame [*cf.* equation (14)] will be used in the following.

By defining the transformation (rotation) matrix Ω , transforming from the (orthonormal) crystal frame of reference C to the specimen frame of reference S, the compliance tensor s_{ijkl}^S can be expressed in terms of the compliance tensor in the (orthonormal) crystal reference frame s_{ijkl}^C , of which the components are tabulated in various textbooks and databases:

$$s_{ijkl}^S = \Omega_{im} \Omega_{jn} \Omega_{ko} \Omega_{lp} s_{mnop}^C. \quad (85)$$

By insertion of equation (85) into equation (84), the strain can be expressed as

$$\varepsilon_{\varphi\psi} = m_i^S m_j^S \Omega_{im} \Omega_{jn} \Omega_{ko} \Omega_{lp} s_{mnop}^C \sigma_{kl}^S, \quad (86)$$

which is the basic relation for diffraction stress analysis according to the crystallite group method.

The measurement of the lattice strain of a crystallite group using a particular hkl reflection is not possible for all combinations of φ and ψ . As the diffraction vector has to be oriented perpendicular to the $\{hkl\}$ planes to obtain diffracted intensity, an hkl reflection can only be found for certain combinations of φ and ψ , which are prescribed by the crystal structure of the material and the orientation of the crystallite group under investigation with respect to the specimen frame of reference. On the one hand, this appears to be a limitation of the method as the number of lattice strain measurements is limited to a number of particular hkl reflections and orientations. On the other hand, it is thus also possible to measure the lattice strains for different crystallite groups in a specimen separately, provided that enough hkl , φ and ψ combinations that are unique for only one of the crystallite groups of the specimen are indicated.

Because the components of the diffraction vector in the specimen reference frame contain the factors $\sin \psi$ and $\cos \psi$ [*cf.* equation (14)], the orientation dependence of the lattice strain is, as in the macroscopically elastically isotropic and quasi-isotropic cases, dependent on the geometrical factors $\sin \psi \cos \psi = \frac{1}{2} \sin(2\psi)$ and/or $\sin^2 \psi$.

Two approaches to the stress determination by diffraction on the basis of equation (86) are indicated.

Hauk & Vaessen (1985) (see also Hauk, 1986; Hauk & Oudelhoven, 1988) used analytical simplifications of equation (86) assuming: (i) a principal stress state (*i.e.* all off-diagonal elements of the stress tensor expressed in the specimen reference frame are zero) and (ii) cubic crystal symmetry. In this case, the three unknown components (the principal components) of the stress tensor can be determined from measurements of the diffraction strain for $\varphi = 0$ and 90° by fitting of straight lines or elliptical curves using the stress tensor components as fit parameters such that the strains calculated from equation (86) match the measured strains, *i.e.* by minimizing χ^2 defined by equation (77).

Ligot *et al.* (2004) suggested using equation (86) in a numerical procedure such that computational evaluation without analytical simplifications is possible. In this approach, it is unnecessary to restrict the stress state to a principal stress state or to limit the analysis to cubic crystal symmetry. Hence, now six unknown tensor components can be obtained by fitting the calculated strains using equation (86) to the measured strains employing a least-squares minimization, *i.e.* by minimizing χ^2 defined by equation (77). An additional advantage of this approach is that the lattice strain measurements need not be limited to certain specific orientations, as given by $\varphi = 0$ and 90° .

For polycrystalline specimens, the description of a (possibly complex) texture in terms of a number of ideal orientations is always a simplification: a continuous averaging of stress and strain tensors in Euler space is replaced by a summation over discrete ideal orientations only. For the stress tensor of the specimen, for example, this simplification reads

$$\langle \sigma \rangle = \int \int \int_G f(\mathbf{g}) \sigma(\mathbf{g}) d^3 g \xrightarrow{\text{CGM}} \langle \sigma \rangle = \sum_{\alpha} f_{\alpha} \langle \sigma_{\alpha} \rangle, \quad (87)$$

where f_{α} is the volume fraction of crystallites having a particular ideal orientation, thus forming the crystallite group α (greek symbols are used to avoid confusion with indices of tensors, see equations below) and $\langle \sigma_{\alpha} \rangle$ is the average stress tensor of this crystallite group.

In practice, also crystals exhibiting a (certain) small deviation of their orientation from the ideal orientation are (have to be) incorporated in the corresponding crystallite group. Obviously, the approximation involved in replacing an average in Euler space by a sum over discrete orientations is the less severe the sharper the texture. However, not only the non-ideality of the texture but also the type of grain interaction acting in the specimen influences the severity of the approximation involved in equation (87): only if the grain interaction were of the Reuss type (all crystallites have the same stress state) or if the specimen were to consist of only one particular crystallite group, would equation (87) not be an approximation. It has been demonstrated by Welzel & Mittemeijer (2004) that additional errors can arise in the case of non-ideal textures due to the impossibility to measure lattice strains for individual crystallite groups separately.

Thus, it is generally not possible to estimate straightforwardly the errors involved in employing equation (87) for diffraction stress analysis.

5.3.1. Example. The following calculated example illustrates the use of the crystallite group method in diffraction stress analysis.

Mechanical (lattice) strains of the $\{211\}\langle\bar{1}11\rangle$ crystallite group in a copper specimen, subjected to a biaxial stress state, where $\langle\sigma_{11}^S\rangle = 100$ MPa and $\langle\sigma_{22}^S\rangle = 200$ MPa, are presented in Fig. 15 as a function of $\sin^2\psi$. The mechanical strain was calculated using equation (86) (with single-crystal elastic constants of copper) along three different directions, characterized by the rotation angle φ equal to 0, 74.77 and 90°, respectively.

A measurement of the lattice (mechanical) strain of this crystallite group is possible only for certain combinations of the reflection (hkl) and the sample tilt (ψ) and rotation (φ) angles. The strain data points which could be measured by diffraction are marked by the symbols in Fig. 15. From these lattice strains, if determined in a real measurement, the (unknown) stress tensor components can be obtained on the basis of equation (77) by fitting the calculated strains to the measured strains [using equation (86) for the strain calculation].

Note that non-linear elliptic $\sin^2\psi$ plots, as occur here, are not necessarily an indication of the presence of shear stresses, as would be the case for macroscopically isotropic specimens; texture alone can cause this type of non-linearity (as is the case here).

5.4. Concluding remarks

Both methods presented in §5 have their specific advantages and limitations. The general analysis presented in §5.2 can be applied to (in addition) all textured specimens. In addition to the unknown stress tensor components, information about the elastic grain interaction in the specimen can be obtained (*cf.* §5.2.2). The analysis requires knowledge of the orientation

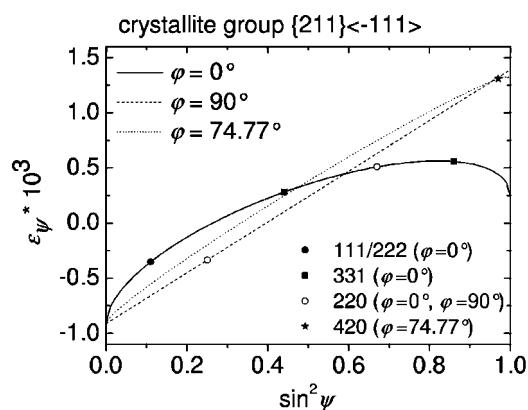


Figure 15

Illustration of the crystallite group method: calculated example. $\sin^2\psi$ plots for the mechanical (lattice) strain for the crystallite group $\{211\}\langle\bar{1}11\rangle$ in a copper specimen subjected to a plane biaxial state of stress with $\sigma_{11}^S = 100$ MPa, $\sigma_{22}^S = 200$ MPa for three values of φ (lines). The symbols indicate at which combinations of tilt (ψ) and rotation (φ) angles the measurement of the lattice strain by diffraction is possible. As an example, the lattice strain can be measured at $\sin^2\psi = 0.25$ and $\varphi = 90^\circ$, and at $\sin^2\psi = 0.67$ and $\varphi = 0^\circ$ employing the 220 reflection.

distribution function, calculation of diffraction stress factors (*cf.* Appendix A) and non-linear least-squares fitting. The crystallite group method presented in §5.3 should be considered as a simplification of the general method for (only) specimens exhibiting a crystallographic texture, which, furthermore, is both strong and sharp. This analysis is simple and easily applicable: linear or elliptic curve fitting generally suffices instead of non-linear least-squares fitting. The crystallite group method requires a rather small number of lattice strains measured at the intensity poles of the texture. However, if the texture of the specimen is not sufficiently sharp or consists of multiple components, application of this method can give rise to significant errors, which cannot be recognized without further ado.

Future research activities are required in particular for the stress analysis of thin films and thin surface regions of bulk polycrystals with respect to the occurrence of anisotropic grain interaction. Origins of anisotropic grain interaction are surface anisotropy and morphological (grain-shape) texture (*cf.* Appendix A). Experimental investigation of diffraction stress factors will be indispensable for the validation of grain-interaction models.

APPENDIX A

Grain-interaction models

Methods for diffraction stress analysis have been discussed in §§4 and 5. For the practical application of any method, the knowledge of diffraction (X-ray) elastic constants (for macroscopically elastically isotropic specimens) or diffraction (X-ray) stress factors (for macroscopically elastically anisotropic specimens) is a prerequisite. Although a measurement of diffraction (X-ray) elastic constants or diffraction (X-ray) stress factors is possible by applying a known load stress to a specimen under simultaneous lattice strain measurement in a diffractometer, this approach is cumbersome and rarely used. Generally, diffraction as well as macroscopic elastic constants are calculated from single-crystal elastic constants by adopting a grain-interaction model.

The basics common to all those grain-interaction models considered are as follows (an exception is the Eshelby–Kröner grain-interaction model and the reader is referred to §A3 for details). For each crystallite, the stress and strain tensors in the specimen reference frame are related by Hooke's law:

$$\varepsilon_{ij}^S = s_{ijkl}^S \sigma_{kl}^S. \quad (88)$$

In equation (88), the s_{ijkl}^S denote the single-crystal elastic compliances expressed in the sample frame of reference. Equation (88) represents a system of nine equations in eighteen components, but as the strain and stress tensors are symmetric (*i.e.* $\varepsilon_{ij} = \varepsilon_{ji}$ and $\sigma_{ij} = \sigma_{ji}$), equation (88) is a short notation for six independent equations with twelve independent unknowns. If six components of the twelve unknowns are known, the other six components can be calculated by solving the system of equations (88). In the different types of grain-interaction model considered here, a total of six stress and/or

strain tensor components in the specimen frame of reference are taken to be equal to the mechanical averages for all crystallites and thus the other six (unknown) components for a crystallite can be calculated from the system of equations (88).

In the following, the commonly used grain-interaction models are discussed and the basic equations necessary for calculating diffraction (X-ray) elastic constants and diffraction (X-ray) stress factors are given. For experimental investigations of diffraction elastic constants and validations of different grain-interaction models, the reader is referred to *e.g.* Brakman *et al.* (1988, Neerfeld–Hill model), Serruys *et al.* (1987, 1989, Neerfeld–Hill model), Hauk & Nikolin (1989, Eshelby–Kröner model), Behnken & Hauk (1991, Eshelby–Kröner model) and Welzel *et al.* (2003, effective grain-interaction model for thin films).

A1. The Voigt model

The assumption for grain interaction in the Voigt model (Voigt, 1910) is that the strain distribution is homogeneous in the specimen, *i.e.* the strain tensor ε^S is the same for all crystallites. This assumption implies that the aggregate remains coherent when it is strained, since all crystallites are deformed in exactly the same way. Thus, there is continuity of the strain at the grain boundaries. As a consequence, the stress tensor is different in each (differently oriented) crystallite. The resulting discontinuities of the stress at the grain boundaries violate mechanical equilibrium. As a consequence, this grain-interaction model is generally not compatible with the mechanical behaviour of real polycrystals. However, the Voigt model is important in the context of effective grain-interaction models (see §A5).

The X-ray stress factors can be calculated (see, for example, Hauk, 1997) as follows:

$$F_{ij}(\psi, \varphi, hkl) = m_k^S \frac{\int_0^{2\pi} (c^S(hkl, \lambda, \varphi, \psi))_{ijkl}^{-1} f^*(hkl, \lambda, \varphi, \psi) d\lambda}{\int_0^{2\pi} f^*(hkl, \lambda, \varphi, \psi) d\lambda} m_l^S \quad (89)$$

In equation (89), c^S denotes the single-crystal elastic stiffness tensor expressed in the sample frame of reference. In the absence of texture [$f^*(hkl, \lambda, \varphi, \psi) \equiv 1$], the polycrystal is macroscopically elastically isotropic, and thus the X-ray elastic constants S_1^{hkl} and $\frac{1}{2}S_2^{hkl}$ can be used instead of the stress factors.

For cubic crystal symmetry, for example, the X-ray elastic constants S_1 and $\frac{1}{2}S_2$ [*cf.* also equation (82) for the relation of the X-ray stress factors to the X-ray elastic constants] can be calculated from the components of the single-crystal compliance tensor according to (Voigt, 1910; Reuss, 1929):

$$S_1 = \frac{2s_0(s_{11} + 2s_{12}) + 5s_{12}s_{44}}{6s_0 + 5s_{44}} \quad (90)$$

and

$$\frac{1}{2}S_2 = \frac{5(s_{11} - s_{12})s_{44}}{6s_0 + 5s_{44}} \quad (91)$$

with

$$s_0 = s_{11} - s_{12} - s_{44}/2. \quad (92)$$

Note that the XECs, according to the Voigt model, do not depend on hkl and thus are equal to the mechanical constants.

A2. The Reuss model

The assumption for grain interaction in the Reuss model (Reuss, 1929) is that the stress distribution is homogeneous in the specimen, *i.e.* the stress tensor σ^S is equal for all crystallites. As a consequence, the strain tensor is different in each crystallite. This assumption implies that strain mismatch occurs at grain boundaries. As a consequence, this grain-interaction model is generally not compatible with the mechanical behaviour of real polycrystals. However, the Reuss model is important in the context of effective grain-interaction models (see §A5).

The X-ray stress factors can be calculated (see, for example, Hauk, 1997) as follows:

$$F_{ij}(\psi, \varphi, hkl) = m_k^S \frac{\int_0^{2\pi} s^S(hkl, \lambda, \varphi, \psi)_{ijkl} f^*(hkl, \lambda, \varphi, \psi) d\lambda}{\int_0^{2\pi} f^*(hkl, \lambda, \varphi, \psi) d\lambda} m_l^S \quad (93)$$

In the absence of texture [$f^*(hkl, \lambda, \varphi, \psi) \equiv 1$], the polycrystal is macroscopically elastically isotropic, and thus the X-ray elastic constants S_1^{hkl} and $\frac{1}{2}S_2^{hkl}$ can be used instead of the stress factors.

For cubic crystal symmetry, for example, the X-ray elastic constants S_1^{hkl} and $\frac{1}{2}S_2^{hkl}$ can be calculated from the components of the single-crystal compliance tensor according to (Möller & Martin, 1939)

$$S_1^{hkl} = s_{12} + s_0 \Gamma(hkl) \quad (94)$$

and

$$\frac{1}{2}S_2^{hkl} = s_{11} - s_{12} - 3s_0 \Gamma(hkl), \quad (95)$$

where $\Gamma(hkl)$ is the orientation factor for cubic materials:

$$\Gamma(hkl) = (h^2k^2 + h^2l^2 + k^2l^2)/(h^2 + k^2 + l^2)^2. \quad (96)$$

Note that the XECs according to the Reuss model are hkl dependent.

A3. The Eshelby–Kröner model

In this model, the crystallites surrounding an individual crystallite are conceived, in a statistical sense, as an elastically homogenous matrix with the elastic properties of the entire polycrystal. This model involves the solution of a so-called inclusion problem (Eshelby, 1957), where the stress/strain fields inside an inclusion embedded in a homogeneous matrix have to be calculated on the basis of the underlying differential equations of the anisotropic elasticity theory. Rigorous analytical solutions are only available for the case that the

matrix is elastically isotropic, the inclusion has a spherical shape and the elastic properties of the inclusion exhibit cubic symmetry (Kröner, 1958). The model was extended to the case of crystallographically textured specimens by Kneer (1965). The calculation in this case involves a spherical anisotropic inclusion embedded in an elastically anisotropic matrix and analytical solutions are no longer feasible. Instead, an iterative numerical procedure has to be employed.

The basics are as follows. The elastic strain of a single-crystalline inclusion (grain) in a polycrystalline aggregate can be expressed as

$$\varepsilon_{ij}(\alpha, \beta, \gamma) = [S_{ijkl} + t_{ijkl}(\alpha, \beta, \gamma)]\langle\sigma_{kl}\rangle. \quad (97)$$

Obviously, the tensor t accounts for the deviation of the elastic properties of an individual grain from the (average) elastic properties of the entire polycrystal/surrounding matrix [*cf.* equation (88)]. In this view, $t(\sigma)$ is a strain in the individual crystallite induced by the mismatch of the elastic constants of a crystallite with respect to those of the matrix to be added to the matrix-average strain contribution $S(\sigma)$ to arrive at the total strain ε of the crystallite. The tensor t depends on the shape of the inclusion, the single-crystal elastic constants and the macroscopic mechanical compliance tensor S of the aggregate. Usually, spherical inclusions are considered; this is a valid assumption for the case of polycrystals consisting of (on the average) equi-axed grains. For the case of a morphological (grain-shape) texture, *e.g.* ellipsoidal inclusions, all with the same shape orientation, see Koch *et al.* (2004). Note that, considering a morphological (grain-shape) texture, the Eshelby–Kröner model becomes a direction-dependent grain-interaction model, *i.e.* the grain-interaction assumptions along different directions in the specimen are inequivalent; for details, see Welzel, Freour & Mittemeijer (2004).

Averaging equation (97) over the entire specimen results in

$$\langle\varepsilon_{ij}\rangle = S_{ijkl}\langle\sigma_{kl}\rangle = \langle S_{ijkl} + t_{ijkl}(\alpha, \beta, \gamma)\rangle\langle\sigma_{kl}\rangle \quad (98)$$

and thus it must hold that

$$\langle t \rangle = 0. \quad (99)$$

Generally, the components of the mechanical compliance tensor S are, based on starting values, varied in an iteration procedure until t satisfies the boundary condition expressed by equation (99). Then, the X-ray stress factors can be calculated from the thus determined values for S (see, for example, Hauk, 1997) as follows:

$$F_{ij}(\psi, \varphi, hkl) = m_k^S \left\{ \int_0^{2\pi} [S^S(hkl, \lambda, \varphi, \psi)_{ijkl} + t^S(hkl, \lambda, \varphi, \psi)_{ijkl}] \times f^*(hkl, \lambda, \varphi, \psi) d\lambda \Big/ \int_0^{2\pi} f^*(hkl, \lambda, \varphi, \psi) d\lambda \right\} \times m_l^S. \quad (100)$$

In the absence of crystallographic [$f^*(hkl, \lambda, \varphi, \psi) \equiv 1$] and morphological (grain-shape) texture, the polycrystal is macroscopically elastically isotropic, and thus the X-ray elastic constants S_1^{hkl} and $\frac{1}{2}S_2^{hkl}$ can be used instead of the stress factors.

For a crystallographically and morphologically untextured (*i.e.* macroscopically elastically isotropic) specimen composed of cubic crystallites, the XECs can be calculated from (Bollenrath *et al.*, 1967)⁴

$$S_1(hkl) = S_{12} + T_{12} + T_0 \Gamma(hkl) \quad (101)$$

and

$$\frac{1}{2}S_2(hkl) = S_{11} - S_{12} + T_{11} - T_{12} - 3 T_0 \Gamma(hkl) \quad (102)$$

with

$$T_0 = T_{11} - T_{12} - 2T_{44} \quad (103)$$

and

$$\Gamma(hkl) = (h^2k^2 + k^2l^2 + l^2h^2)/(h^2 + k^2 + l^2)^2. \quad (104)$$

T_{11} and T_{12} can be calculated from

$$T_{11} - T_{12} = \frac{(G - \nu)(3K + 6G)}{G[8G^2 + G(9K + 12\nu) + 6\nu K]} \quad (105)$$

and

$$2T_{44} = \frac{(G - \mu)(3K + 6G)}{G[8G^2 + G(9K + 12\mu) + 6\mu K]} \quad (106)$$

with

$$3K = 1/(S_{11} + 2S_{12}), \quad (107)$$

where K is the bulk modulus,

$$\mu = 1/S_{44} \quad (108)$$

and

$$2\nu = 1/(S_{11} - S_{12}). \quad (109)$$

The shear modulus G can be obtained as the solution of the following equation:

$$G^3 + \alpha G^2 + \beta G + \gamma = 0, \quad (110)$$

where the following abbreviations have been used:

$$\alpha = (9K + 4\nu)/8, \quad (111)$$

$$\beta = -(3K + 12\nu)\mu/8 \quad (112)$$

and

$$\gamma = -3K\nu\mu/4. \quad (113)$$

A4. The Vook–Witt and inverse Vook–Witt models

In a bulk specimen, each crystallite is surrounded by other crystallites in three dimensions. In films, which often have a columnar grain structure, each surface-adjacent crystallite is surrounded by other crystallites in only two dimensions. Owing to their microstructure and reduced dimensionality, thin films cannot generally be considered as macroscopically elastically isotropic. Rather they can exhibit macroscopically transversely isotropic properties [even in the absence of

⁴ Note that the symbols α , β , γ , μ and ν bear no relation to the same symbols used in earlier sections. These symbols are used here for consistency with the cited literature.

crystallographic texture (van Leeuwen *et al.* 1999)]. The traditional models for grain interaction [Voigt, Reuss, Eshelby–Kröner (involving spherical inclusions; *cf.* §A3), Neerfeld–Hill] are compatible only with macroscopically isotropic elastic properties (in the absence of crystallographic texture) and are thus inappropriate for the analysis of stress in thin films.

In the bulk of a polycrystal, with respect to grain interaction, generally all (principal) directions are equivalent. For this reason, the number of grain-interaction models of extreme types of grain-interaction assumptions is two for bulk materials (Reuss and Voigt, provided that all directions within the bulk are equivalent for grain interaction). Columnar thin films possess two principal directions exhibiting possibly different types of grain interactions: the in-plane direction (all in-plane directions are equivalent) and the direction perpendicular to the surface of the film. On the basis of the same reasoning, four types of extreme grain-interaction models can then be formulated for columnar thin films, as two principal directions, each with two possible extreme grain interactions, occur. The Voigt and Reuss models have already been discussed (§§A1 and A2). The two additional extreme grain-interaction models are the Vook–Witt and inverse Vook–Witt models. Such models, adopting different grain-interaction assumptions along different (principal) directions in the specimen, are called direction-dependent grain-interaction models.

A4.1. The Vook–Witt model. Vook & Witt (1965) have proposed a set of grain-interaction assumptions which reflect transverse isotropy and thus may be applicable to thin films [see van Leeuwen *et al.* (1999) for the case of untextured specimens, and Leoni *et al.* (2001) for the case of (fibre-) textured specimens]. An (at least) macroscopically elastically transversely isotropic specimen subjected to a planar rotationally symmetric state of stress is considered [for a generalization to any stress state, see Welzel & Freour (2004)]. The grain-interaction assumptions of the Vook–Witt model are then: (i) the strain is rotationally symmetric in the plane of the film and (ii) equal for all crystallites (Voigt-type grain interaction), and (iii) the stresses perpendicular to the layer are zero for all crystallites (Reuss-type grain interaction), *i.e.* the crystallites can deform freely in this direction. These assumptions fix parts of the stress and strain tensor for all crystallites:

$$\varepsilon^S = \begin{pmatrix} \varepsilon_{\parallel}^S & 0 & \circ \\ 0 & \varepsilon_{\parallel}^S & \circ \\ \circ & \circ & \circ \end{pmatrix} \quad (114)$$

and

$$\sigma^S = \begin{pmatrix} \circ & \circ & 0 \\ \circ & \circ & 0 \\ 0 & 0 & 0 \end{pmatrix}. \quad (115)$$

The tensor components marked by \circ are not explicitly specified for every crystallite, but these components can be calculated from Hooke’s law for every crystallite according to equation (88). Thus, for a particular value of the strain parallel

to the substrate $\varepsilon_{\parallel}^S$, all non-zero strain and stress tensor components can be calculated by solving the system of equations (88) (for explicit equations, see Leoni *et al.*, 2001).

The Vook–Witt grain-interaction model may be more appropriate for the analysis of macroscopic stress in thin films than traditional grain-interaction models (such as the Reuss or Voigt models). A remarkable feature of this grain-interaction model is that, even in the *absence of crystallographic texture*, the $\sin^2\psi$ plots are non-linear (van Leeuwen *et al.*, 1999; see also §5.2.1).

A4.2. The inverse Vook–Witt model. The inverse Vook–Witt model completes the set of four extreme grain-interaction models for (columnar) thin films. As for the Vook–Witt model, a transversely isotropic specimen subjected to a planar rotationally symmetric state of stress is considered [for a generalization to any stress state, see Welzel & Freour (2004)]. The grain-interaction assumptions are as follows: (i) the in-plane stress is rotationally symmetric and (ii) equal for all crystallites (Reuss-type grain interaction), and (iii) the strain perpendicular to the film surface is equal for all crystallites (Voigt-type grain interaction). Like in the (regular) Vook–Witt model, these assumptions fix certain strain and stress tensor components for all crystallites [*cf.* equations (114) and (115)]:

$$\varepsilon^S = \begin{pmatrix} \circ & \circ & 0 \\ \circ & \circ & 0 \\ 0 & 0 & \varepsilon_{\perp}^S \end{pmatrix} \quad (116)$$

and

$$\sigma^S = \begin{pmatrix} \sigma_{\parallel}^S & 0 & \circ \\ 0 & \sigma_{\parallel}^S & \circ \\ \circ & \circ & \circ \end{pmatrix}. \quad (117)$$

The missing strain and stress tensor components for each crystallite, marked by \circ , can be calculated by solving the system of equations (88).

The inverse Vook–Witt grain-interaction model is required for the construction of an effective grain-interaction model for thin films (see §A5). A remarkable feature of this grain-interaction model is that, as for the Vook–Witt model, *even in the absence of crystallographic texture*, the $\sin^2\psi$ plots are non-linear (Welzel *et al.*, 2003).

A5. Effective grain-interaction models

The mechanical elastic constants, the X-ray elastic constants and the X-ray stress factors calculated employing extreme grain-interaction models are generally not compatible with the real elastic behaviour of polycrystals. However, it is often found empirically that averaging the elastic constants of extreme grain-interaction models results in elastic data that are compatible with experimentally determined values. The background of any averaging of (extreme) grain-interaction models to represent physical reality could be described as follows. A real sample is conceived to be constituted by separate volume fractions of crystallites, each of which obeys a certain type of grain interaction. For the following discussion,

an average of (extreme) grain-interaction models will be called an effective grain-interaction model. Depending on the type of specimen considered, appropriate choices of the grain-interaction models 'to be averaged' can be made.

Under the assumption that a volume fraction f_i of the polycrystalline aggregate obeys the (extreme) grain-interaction model i , average elastic constants can be calculated as an arithmetic average:

$$\Xi = \sum_i f_i \Xi_i, \quad (118)$$

where Ξ stands for a certain elastic constant (*e.g.* Young's modulus or an X-ray elastic constant) and

$$\sum_i f_i = 1. \quad (119)$$

A5.1. The Neerfeld–Hill model. The Voigt and Reuss models are the extreme cases of grain interaction in bulk polycrystals: either the strain tensor (Voigt model) or the stress tensor (Reuss model) for each crystallite is assumed to be equal to the mechanical strain or stress tensor, respectively; they are therefore incompatible with physical reality because of the corresponding stress, respectively strain discontinuities at the grain boundaries. It was shown that the Voigt and Reuss models set bounds for the mechanical elastic constants (Hill, 1952). Further, Neerfeld (1942) and Hill (1952), on an empirical basis, suggested that the arithmetic (or geometric⁵; Hill, 1952) average of X-ray (Neerfeld, 1942) and macroscopic (Neerfeld, 1942; Hill, 1952) elastic constants calculated according to the models of Voigt and Reuss, respectively, are in better agreement with experimental data. This approach is referred to as the Neerfeld–Hill model.

Generally, an arithmetic average where the Voigt and Reuss contributions are both 1/2 is adopted (however, other weighing schemes for the two extreme models could be conceived):

$$\Xi_{\text{NH}} = f \Xi_{\text{R}} + (1 - f) \Xi_{\text{V}} \quad (120)$$

where Ξ stands for a certain elastic constant (*e.g.* Young's modulus or an X-ray elastic constant), the subscripts indicate the grain-interaction models and f is a mixing parameter (corresponding to the volume fraction of crystallites obeying the Reuss model). This parameter may be used as an additional fit parameter in a general least-squares analysis (*cf.* §§4.3 and 5.2; see also Serruys *et al.*, 1987, 1989).

A5.2. An effective grain-interaction model for thin films. Even though the Vook–Witt and inverse Vook–Witt grain-interaction models can be considered as 'intermediate' models of grain interaction (with reference to the extreme Voigt and Reuss models), these models still involve extreme grain-interaction assumptions along the two considered principal directions.

⁵ Usually the arithmetic and not the geometric average is used. The geometrical average of n numbers is defined as the n th root of the product of the numbers. For Young's modulus, as an example, the geometric average of the moduli according to the Reuss (E_{R}) and Voigt (E_{V}) models E_{GA} is defined as $(E_{\text{R}}E_{\text{V}})^{1/2}$.

An effective grain-interaction model for a thin film or, possibly, for surface-adjacent material can be constructed (Welzel *et al.*, 2003). Consider the following example. The Reuss model can be combined with the Vook–Witt model by assuming that the specimen is composed of an effective volume fraction f_{R} of the sample obeying the Reuss model and an effective volume fraction f_{VW} obeying the Vook–Witt model. Such a combined model leads, effectively, to partial in-plane Reuss behaviour: whereas the crystallites are tightly connected together with respect to the in-plane direction in the Vook–Witt approach and exhibit identical strains, the combination with the Reuss constraint gives the crystallites some degree of freedom for in-plane deformation independent of the neighbouring crystallites, thereby lifting the (unrealistic) constraint of identical planar strain for every crystallite. A similar discussion can be given for combinations of other extreme grain-interaction models.

A quantification of the effect of model mixing on the grain interaction can be achieved by defining interaction parameters for the two principal directions.

(i) In-plane interaction parameter w_{\parallel} : equals one for a Voigt-type interaction (crystallites are tightly connected together) and zero for a Reuss-type interaction (crystallites can deform independently of neighbouring crystallites, but their stresses are identical).

(ii) The out-of-plane interaction parameter w_{\perp} : definition analogous to the in-plane parameter w_{\parallel} , *i.e.* w_{\perp} equals one for Voigt-type interaction and zero for a Reuss-type interaction.

Combining the models for extreme types of grain interaction, results in average values $\langle w_{\parallel} \rangle$ and $\langle w_{\perp} \rangle$ for the interaction parameters:

$$\langle w_{\parallel} \rangle = \sum_i f_i w_{\parallel,i} \quad (121)$$

and

$$\langle w_{\perp} \rangle = \sum_i f_i w_{\perp,i}. \quad (122)$$

In equations (121) and (122), the f_i represent, as in equation (118), effective volume fractions of grains obeying the grain-interaction model i . For a given combination of grain-interaction models, the average interaction parameters can be calculated following equations (121) and (122).

Generally, the parameters f_i are not known *a priori*. In this case, the parameters f_i may be used as additional fit parameters in a general least-squares analysis (*cf.* §§4.3 and 5.2; see also Welzel *et al.*, 2003).

References

- Acker, K. van, de Buysier, L., Celis, J. P. & van Houtte, P. (1994). *J. Appl. Cryst.* **27**, 56–66.
- Ballard, B. L., Predecki, P. K., Watkins, T. R., Kozaczek, K. J., Braski, D. N. & Hubbard, C. R. (1997). *Adv. X-ray Anal.* **39**, 363–370.
- Baron, H. U. & Hauk, V. (1988). *Z. Metallkd.* **79**, 41–49, 127–131.
- Behnken, H. & Hauk, V. (1991). *Z. Metallkd.* **82**, 151–158.
- Behnken, H. & Hauk, V. (2000). In *Proceedings of ICRS6*, 10–12 July 2000, Oxford, pp. 277–282. London: IOM Communications.
- Bollenrath, F., Hauk, V. & Müller, E. H. (1967). *Z. Metallkd.* **58**, 76–82.

- Bollenrath, F., Osswald, E., Möller, H. & Neerfeld, H. (1941). *Arch. Eisenhüttenwesen*, **15**, 183–194.
- Brakman, C. M. (1983). *J. Appl. Cryst.* **16**, 325–340.
- Brakman, C. M., de Keijser, Th. H., van der Pers, N. M., Penning, P. & Radelaar, S. (1988). *Philos. Mag. A*, **58**, 635–60.
- Bunge, H.-J. (1982). *Texture Analysis in Materials Science*. London: Butterworths.
- Christenson, A. L. & Rowland, E. S. (1953). *Trans. ASM*, **45**, 638–676.
- Delhez, R., de Keijser, Th. H. & Mittemeijer, E. J. (1982). *Fresen. Z. Anal. Chem.* **312**, 1–16.
- Delhez, R., de Keijser, Th. H. & Mittemeijer, E. J. (1987). *Surf. Eng.* **3**, 331–342.
- Dölle, H. (1979). *J. Appl. Cryst.* **12**, 489–501.
- Dölle, H. & Hauk, V. (1976). *Härt.-Tech. Mitt.* **31**, 165–168.
- Dölle, H. & Hauk, V. (1978). *Z. Metallkd.* **69**, 410–417.
- Dölle, H. & Hauk, V. (1979). *Z. Metallkd.* **70**, 682–685.
- Dümmer, T., Eigenmann, B., Stüßler, M., Leiste, H., Löhe, D., Müller, H. & Vöhringer, O. (1999). *Z. Metallkd.* **90**, 780–787.
- Eigenmann, B. & Macherauch, E. (1995). *Mater.-Wiss. u. Werkstofftech.* **26**, 148–160, 199–216.
- Eigenmann, B. & Macherauch, E. (1996). *Mater.-Wiss. u. Werkstofftech.* **27**, 426–437, 491–501.
- Eigenmann, B., Scholtes, B. & Macherauch, E. (1992). *Residual Stresses III*, edited by H. Fujiwara, T. Abe & K. Tanaka, pp. 601–606. Amsterdam: Elsevier Applied Science.
- Eshelby, J. D. (1957). *Proc. R. Soc. A*, **241**, 376–396.
- Evenschor, P. D. & Hauk, V. (1975). *Z. Metallkd.* **66**, 167–168.
- Giacovazzo, C., Monaco, H. L., Votterbo, D., Scordari, F., Gilli, G., Zanotti, G. & Catti, M. (1998). *Fundamentals of Crystallography*. Oxford: Oxford Science.
- Genzel, Ch. (1994). *Phys. Status Solidi A*, **146**, 629–637.
- Genzel, Ch. (1997). *Phys. Status Solidi A*, **159**, 283–296.
- Genzel, Ch. (1999). *J. Appl. Cryst.* **32**, 770–778.
- Genzel, Ch., Broda, M., Dantz, D. & Reimers, W. (1999). *J. Appl. Cryst.* **32**, 779–787.
- Hauk, V. (1952). *Arch. Eisenhüttenwesen*, **23**, 353–361.
- Hauk, V. (1986). *Adv. X-ray Anal.* **29**, 1–15.
- Hauk, V. (1995). *Härt.-Tech. Mitt.* **50**, 138–144.
- Hauk, V. (1997). Editor. *Structural and Residual Stress Analysis by Nondestructive Methods*. Amsterdam: Elsevier.
- Hauk, V. & Krüger, B. (2000). *Mater. Sci. Eng. A*, **284**, 261–267.
- Hauk, V. & Nikolin, H.-J. (1989). *Z. Metallkd.* **80**, 862–872.
- Hauk, V. & Oudelhoven, R. (1988). *Z. Metallkd.* **79**, 41–49.
- Hauk, V. & Vaessen, G. (1985). *Z. Metallkd.* **76**, 102–107.
- Hill, R. (1952). *Proc. Phys. Soc. London*, **65**, 349–354.
- Hoffman, R. W. (1966). *The Mechanical Properties of Thin Condensed Films*, in *Physics of Thin Films*, Vol. 3, edited by G. Hass & R. E. Thun, pp. 211–273. New York: Academic Press.
- Hoffman, R. W. (1976). *Mechanical Properties of Non-Metallic Thin Films*, in *Physics of Non-Metallic Thin Films*, edited by C. H. S. Dupuy & A. Cachard, *Proceedings NATO Advanced Study Institutes Series, Series B: Physics*, Vol. 14, pp. 273–353. New York: Plenum Press.
- Kamminga, J. D., Delhez, R., de Keijser, Th. H. & Mittemeijer, E. J. (2000a). *J. Appl. Cryst.* **33**, 108–111.
- Kamminga, J. D., de Keijser, Th. H., Delhez, R. & Mittemeijer, E. J. (2000b). *J. Appl. Cryst.* **33**, 1059–1066.
- Kneer, G. (1965). *Phys. Status Solidi*, **9**, 825–834.
- Koch, N., Welzel, U., Wern, H. & Mittemeijer, E. J. (2004). *Philos. Mag.* **84**, 3547–3570.
- Kröner, E. (1958). *Z. Physik*, **151**, 504–518.
- Leeuwen, M. van, Kamminga, J.-D. & Mittemeijer, E. J. (1999). *J. Appl. Phys.* **86**, 1904–1914.
- Leoni, M., Welzel, U., Lamparter, P., Mittemeijer, E. J. & Kamminga, J.-D. (2001). *Philos. Mag. A*, **81**, 597–623.
- Leoni, M., Welzel, U. & Scardi, P. (2004). *J. Res. Natl Inst. Stand. Technol.* **109**, 27–48.
- Leverenz, T., Eigenmann, B. & Macherauch, E. (1996). *Z. Metallkd.* **87**, 616–625.
- Ligot, J., Welzel, U., Lamparter, P. & Mittemeijer, E. J. (2004). In preparation.
- Lode, W. & Peiter, A. (1981). *Metall*, **35**, 758–762.
- Ma, C.-H., Huang, J.-H. & Chen, H. (2002). *Thin Solid Films*, **418**, 73–78.
- Macherauch, E. & Müller, P. (1961). *Z. Angew. Phys.* **13**, 305–312.
- Macherauch, E., Wohlfahrt, H. & Wolfstieg, U. (1973). *Härt.-Tech. Mitt.* **28**, 201.
- Machlin, E. S. (1995). *Materials Science in Microelectronics*, Vol. 2. New York: Giro Press.
- Marra, W. C., Eisenberger, P. & Cho, A. Y. (1979). *J. Appl. Phys.* **50**, 6927–6933.
- Meyers, M. A. & Chawla, K. K. (1984). *Mechanical Metallurgy, Principles and Applications*. Englewood Cliffs, New Jersey: Prentice-Hall.
- Mittemeijer, E. J. & Scardi, P. (2004). Editors. *Diffraction Analysis of the Microstructure of Materials*. Berlin: Springer.
- Möller, H. & Barbers, J. (1935). *Mitt. K.-Wilh.-Inst. Eisenforsch.* **17**, 157–177.
- Möller, H. & Martin, G. (1939). *Mitt. K.-Wilh.-Inst. Eisenforsch.* **21**, 261–269.
- Neerfeld, H. (1942). *Mitt. K.-Wilh.-Inst. Eisenforsch.* **24**, 61–70.
- Noyan, I. C. & Cohen, J. B. (1987). *Residual Stress. Measurement by Diffraction and Interpretation*. New York: Springer.
- Noyan, I. C., Huang, T. C. & York, B. R. (1995). *Crit. Rev. Solid State Mater. Sci.* **20**, 125–177.
- Nye, J. F. (1957). *Physical Properties of Crystals*. Oxford University Press.
- Ortner, B. (1986a). *Adv. X-ray Anal.* **29**, 113–118.
- Ortner, B. (1986b). *Adv. X-ray Anal.* **29**, 387–394.
- Parrat, L. G. (1954). *Phys. Rev.* **95**, 359–369.
- Predecki, P., Ballard, B. & Zhu, X. (1993). *Adv. X-ray Anal.* **36**, 237–245.
- Press, W. H., Flannery, B. P., Teukolsky, S. A. & Vetterling, W. T. (1986). *Numerical Recipes*. Cambridge University Press.
- Quaeyhaegens, C., Knuyt, G. & Stals, L. M. (1995). *Surf. Coat. Technol.* **74–75**, 104–109.
- Quaeyhaegens, C., Knuyt, G. & Stals, L. M. (1996). *J. Vac. Sci. Technol. A*, **14**, 2462–2468.
- Reuss, A. (1929). *Z. Angew. Math. Mech.* **9**, 49–58.
- Roe, R.-J. & Krigbaum, W. R. (1964). *J. Chem. Phys.* **40**, 2608–2615.
- Serruys, W., Van Houtte, P. & Aernoudt, E. (1987). In *Residual Stresses in Science and Technology*, edited by E. Macherauch & V. Hauk, pp. 417–424. Oberursel: Deutsche Gesellschaft für Metallkunde.
- Serruys, W., Langouche, F., van Houtte, P. & Aernoudt, E. (1989). In *Proceedings of ICRS2*, edited by G. Beck, A. Denis & A. Simon, pp. 166–171. London: Elsevier Applied Science.
- Skrzypek, S. J. & Baczmanski, A. (2001). *Adv. X-ray Anal.* **44**, 134–145.
- Skrzypek, S. J., Baczmanski, A., Ratuszek, W. & Kusior, E. (2001). *J. Appl. Cryst.* **34**, 427–435.
- Somers, M. A. J. & Mittemeijer, E. J. (1990). *Met. Trans. A*, **21**, 189–204.
- Stickforth, J. (1966). *Tech. Mitt. Krupp-Forsch.-Ber.* **24**, 89–102.
- Tamura, N., MacDowell, A. A., Spolenak, R., Valek, B. C., Bravman, J. C., Brown, W. L., Celestre, R. S., Padmore, H. A., Batterman, B. W. & Patel, J. R. (2003). *J. Synchrotron Rad.* **10**, 137–143.
- Toney, M. F. & Brennan, S. (1989). *Phys. Rev. B*, **39**, 7963–7966.
- Vermeulen, A. C. (2000). In *Proceedings of ICRS6*, pp. 283–290. London: IOM Communications.
- Vermeulen, A. C. (2002). *Mater. Sci. Forum*, **404–407**, 35–40.
- Vermeulen, A. C. & Houtman, E. (2000). *Mater. Sci. Forum*, **347–349**, 17–22.
- Voigt, W. (1910). *Lehrbuch der Kristallphysik*. Leipzig: Teubner.
- Vook, R. W. & Witt, F. (1965). *J. Appl. Phys.* **7**, 2169–2171.

- Wagner, C. N. J., Boldrick, M. S. & Perez-Mendez, V. (1983). *Adv. X-ray Anal.* **26**, 275–282.
- Welzel, U. & Freour, S. (2004). In preparation.
- Welzel, U., Freour, S. & Mittemeijer, E. J. (2004). *Philos. Mag.* Submitted.
- Welzel, U., Leoni, M. & Mittemeijer, E. J. (2003). *Philos. Mag.* **83**, 603–630.
- Welzel, U., Leoni, M. & Mittemeijer, E. J. (2004). *Diffraction Analysis of the Microstructure of Materials*, edited by E. J. Mittemeijer & P. Scardi, pp. 363–390. Berlin: Springer.
- Welzel, U. & Mittemeijer, E. J. (2003). *J. Appl. Phys.* **93**, 9001–9011.
- Welzel, U. & Mittemeijer, E. J. (2004). *Mater. Sci. Forum*, **443–444**, 131–134.
- Willemsse, P. F. & Naughton, B. P. (1985). *Mater. Sci. Technol.* **1**, 41–44.
- Willemsse, P. F., Naughton, B. P. & Verbraak, C. A. (1982). *Mater. Sci. Eng.* **56**, 25–37.
- Windischmann, H. (1992). *Crit. Rev. Solid State Mater. Sci.* **17**, 547–596.
- Winholtz, R. A. & Cohen, J. B. (1988). *Aust. J. Phys.* **41**, 189–199.